A UNIFIED METHOD TO PREDICT PILOT-INDUCED OSCILLATIONS

by

Anthony B. Page

Dissertation submitted to the faculty of the

Virginia Polytechnic Institute and State University

in partial fulfillment of the requirements for the degree of

DOCTOR OF PHILOSOPHY

in

Aerospace Engineering

APPROVED:

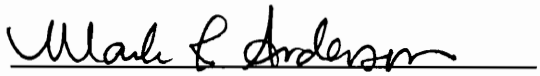

M. R. Anderson, Chairman

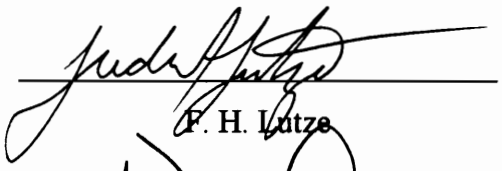

F. H. Lutze

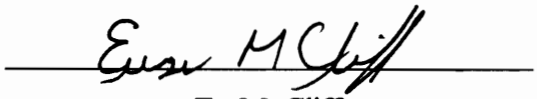

E . M. Cliff

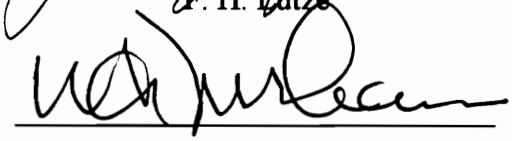

W. C. Durham

H. H. Robertshaw

August 1996

Blacksburg, Virginia

Keywords: Aircraft, Stability, Robustness, Nonlinear, Control

A UNIFIED METHOD TO PREDICT PILOT-INDUCED OSCILLATIONS

by

Anthony B. Page

M. R. Anderson, Chairman

Department of Aerospace Engineering

(ABSTRACT)

A pilot-induced oscillation (PIO) is a dynamic coupling between pilot and aircraft that produces undesired oscillations as a result of attempted pilot control of the vehicle. Present day methods that are intended to predict which aircraft are susceptible to PIO deal primarily with the linear dynamics associated with both the pilot and vehicle. These methods are incapable of handling multiple dynamic effects. An analysis method that is able to handle several dynamic effects simultaneously, including nonlinearities arbitrarily located in both the pilot and vehicle models, is offered. The new unified analysis method draws from recent advances in pilot modeling, stability robustness analysis, and multivariable describing function analysis to solve the problem of identifying aircraft with PIO tendencies. The method handles simultaneous dynamic characteristics as well as nonlinear effects. Control surface rate limiting is one nonlinear effect that is known to contribute to many PIO occurrences. An example analysis of the M2-F2 lifting body is used to demonstrate how several individual dynamic effects can be analyzed simultaneously to predict aircraft PIO susceptibility. In this case, the combined effect of five separate nonlinearities and two linear parameter variations are studied. While the PIO tendency of the M2-F2 is most likely caused by poor flying qualities, a unified PIO analysis shows exactly which dynamic elements couple with the pilot dynamics to cause oscillations. The analysis results show the PIO amplitude and frequency that occurred during flight testing and piloted simulation of the M2-F2 can be accurately predicted assuming a Modified Optimal Control Model of the human pilot and simultaneous limiting in the pilot command and roll feedback channels.

For my children, assuming I ever have any.

Acknowledgements

I am greatly indebted to my major advisor, Mark Anderson, for not only securing the funding for this project, but also for his guidance, encouragement, career advice, and friendship. A special thanks to Fred Lutze, who acted as my advisor for the first four years of my graduate career, for his support and occasional conversation about golf. Many thanks to all the members of my committee, Mark Anderson, Fred Lutze, Gene Cliff, Bull Durham, and Harry Robertshaw, for making the complex understandable and for being a great group of people with whom to be associated personally as well as professionally.

Thanks to my fellow graduate students for their friendship, stimulating conversations, and companionship on the golf course. Thanks to the Department of Aerospace Engineering and to Wright Laboratory for providing the financial support that allowed me to maintain my membership at the Virginia Tech Golf Course while completing my Ph.D.

A very special thanks to my extraordinary wife, Kim, for continuing to follow me wherever my career leads us, for supporting me in everything I do, and for making life fun and exciting. Thanks to my in-laws, Roy, Linda, Karen, and Blake, who have always made me feel like one of the family and for providing many delicious meals. Thanks to my brother, Ernie, for his influence during the formative years of my life, for introducing me to the game of golf, and for having a wonderful wife, Larenda, and children, Julia and Ernie III, whom I adore. Thanks to my true friends, Danny and Camille, who never fail to inject humor into my life. Finally, thanks to my mother and late father for passing on to me the values and strength of character (not to mention genes) that have made me who I am.

Contents

List of Figures

List of Tables

List of Symbols

ALT.....Approach and Landing Tests

A-PC.....Aircraft-Pilot Coupling

LQG.....Linear Quadratic Gaussian

MOCM.....Modified Optimal Control Model

OCM.....Optimal Control Model

PIO.....Pilot-Induced Oscillation

SAS.....Stability Augmentation System

SIDF.....Sinusoidal Input Describing Function

TSIDF.....Two Sinusoid Input Describing Function

A.....Vector of input signal amplitudes

a.....Input/output values for various nonlinear elements

a_n, b_n.....Fourier coefficients

D.....Diagonal scaling matrix

D(s).....Transfer function representation of Pade time delay

e.....Displayed error signal

$\bar{f}$.....Vector of auxiliary characteristic equations

G(s).....Aircraft transfer function

g.....Acceleration due to gravity

g(s).....Arbitrary transfer function

$\bar{H}$.....Vector of homotopy equations

I.....Identity matrix

J.....Optimal control cost function

K.....Arbitrary gain

K_d, $K_{\bar{d}}$.....Proportional plus integral control system gains

K_I.....Interconnect ratio

K_p ..... Pilot gain or Roll rate feedback gain

K_{pilot} ..... Pilot gain

K_r ..... Yaw rate feedback gain

K_u ..... Velocity feedback gain

K_θ ..... Pitch attitude feedback gain

$K_{\dot{\theta}}$ ..... Pitch rate feedback gain

$K_{\dot{\phi}}$ ..... Roll rate feedback gain

k ..... Scaling gain

L ..... Equivalent gain

M(s) ..... Transfer function matrix

m ..... slope

N_{comp} ..... Complementary describing function

N_{given} ..... Given describing function

$N(\alpha,\omega)$ ..... Arbitrary sinusoidal input describing function

P ..... Actuator output limit

P(s) ..... Pilot model transfer function

p ..... Roll rate

q ..... Number of uncertainties

R ..... Actuator rate limit

r ..... Yaw rate

$r_c(s)$ ..... Reference input

S ..... Magnitude slope of frequency response

s ..... Laplace variable

T_1, T_2 or T_{p1}, T_{p2} ..... Lead/lag pilot model parameters

t ..... Time or Independent homotopy parameter

U ..... Unitary matrix

x_a ..... Input signal to aileron rate limiter

x_r ..... Input signal to rudder rate limiter

$x(t)$ ..... Input signal to nonlinear element

Y_c ..... Vehicle transfer function

Y_p ..... Pilot transfer function

$y(t)$ ..... Output signal of nonlinear element

$\bar{z}$ ..... Vector of solution variables

α ..... Angle of attack or Amplitude of input signal

β ..... Sideslip angle

Δ ..... Diagonal matrix of parameter variations or describing functions

$\Delta\Phi$ ..... Phase loss from ω_{180} to $2\omega_{180}$

δ ..... Parameter variation or uncertainty

δ_a ..... Aileron input

δ_c ..... Commanded input

δ_{exact} ..... Variation necessary to cause instability

δ_{LS} ..... Lateral stick input

δ_{RP} ..... Rudder pedal input

ζ_{sp} ..... Short period damping ratio

θ ..... Phase angle of input sinusoid

μ ..... Structured singular value

μ_r ..... Structured singular value for real parameter variations

ρ ..... Control rate weighting or Spectral radius

σ ..... Real perturbation in limit cycle frequency

σ_{max} ..... Maximum singular value

τ ..... Time delay

τ_2 ..... Control system time constant

τ_a, τ_d, τ_s, τ_T ..... Pilot time delays

τ_e ..... Effective pilot/vehicle time delay

τ_p ..... Phase delay parameter

τ_R ..... Actuator time constant

Φ ..... Diagonal permutation matrix

Φ_T ..... Matrix representation of all permutation matrices

ϕ ..... Bank angle

ϕ_1 ..... Phase angle of describing function

ϕ_c ..... Commanded bank angle

ϕ_{error} ..... Bank angle error

ω ..... Frequency

ω_{180} ..... Phase crossover frequency

ω_c ..... Gain crossover frequency

ω_{cr} ..... Critical frequency

ω_{exact} ..... Frequency at which instability occurs

ω_{min} ..... Frequency at which structured singular value inverse is a minimum

ω_{sp} ..... Short period frequency

1 Introduction

Since the dawn of manned flight in the early 1900s, the desire has been to design vehicles that could be controlled by the pilot to meet the objectives of the mission. Mission objectives have evolved over the years. The earliest goals were simply to get the craft airborne and return it safely to the ground. However, present day objectives have grown to include these goals as well as the various precision aerial maneuvers required by modern combat aircraft. As the mission objectives have evolved, the dynamics of the aircraft and the control system have likewise evolved to a high level of complexity and sophistication.

In the early days of manned flight, many of the successful aircraft (including the Wright Flyer of 1903, the World War I vintage Sopwith Camel of Britain, and the JN-4 "Jenny" of the United States) were aerodynamically unstable both longitudinally and laterally [1]. Aerodynamic instability means that the aircraft will diverge from normal flight in the absence of continuous pilot control. The success of these aircraft was then dependent on the efforts of the pilot to stabilize the closed-loop pilot/vehicle system.

However, by the 1930s, a consensus was generally reached within the aerospace community that aircraft should be designed to be inherently stable [1]. By this time, flights had increased in duration and the demands on the pilot to perform peripheral duties had also increased. Because control of an unstable aircraft requires constant pilot control and attention, the pilots of earlier unstable aircraft were not as free to perform other necessary functions such as navigation. The pilots of unstable aircraft were also more vulnerable to fatigue on a long flight. Inherent stability was deemed necessary to reduce pilot workload and stress to levels required for safe flight - especially for the commercial airliners developed at that time (1930s) [1].

While the vehicle itself is now generally designed to exhibit favorable response characteristics, or "flying qualities," the dynamic interaction between the pilot and aircraft can, in some instances, lead to undesirable oscillations. That is, the pilot, using inappropriate

actions, can actually destabilize an otherwise stable aircraft. This phenomenon became known as a pilot-induced oscillation. A pilot-induced oscillation (PIO) can then be defined as an undesirable "sustained or uncontrollable oscillation resulting from the efforts of the pilot to control the aircraft" [2].

Since both the pilot and aircraft are complex nonlinear dynamic systems, the problem of predicting the circumstances under which a PIO is likely to develop can be very difficult. Moreover, Reference [3] states that the interface between man and machine has evolved in complexity such that "human factors limitations" (including PIO) have become the lead cause of aircraft accidents. Therefore, it is becoming increasingly important to determine what conditions can lead a pilot to destabilize the closed-loop pilot/aircraft system.

The existence of PIO phenomena has been recognized since the 1940s [4]. Some of the earliest documented PIOs include those during gliding approach and landing of the XS-1 in 1947 (piloted by Herbert Hoover) and the X-15 in 1959 (piloted by Scott Crossfield) [5]. However, the worst possible result of a PIO is exemplified by the attempted speed record run of a McDonnel Douglas F-4H in 1961. During the flight, as the aircraft reached Mach 1.1, a longitudinal oscillation developed. In less than 2 seconds, as the aircraft moved through three cycles of the oscillation, accelerations of -4 to +14 g were reached [3]. The final result was structural break-up of the aircraft in which both the vehicle and pilot were lost.

As a more detailed example, consider the final flight of the M2-F2 in 1969. The M2-F2 was a small unpowered low lift-to-drag ratio research vehicle typical of a space shuttle configuration. A lateral/directional PIO occurred at the rollout of the turn to final approach. The pilot described the scenario as follows [6]:

> *"In the final approach, as I went into the final turn, I wasn't getting the turn rate I wanted so I turned the interconnect up to 0.45 and then continued to turn. I was well established on my glide, very low angle of attack, picking up my airspeed, and had the feeling that I would land just slightly short of the 2-mile point angling across the runway. Everything was going normally with no problems, then suddenly at 5000 to 7000 feet, with no warning at all, I experienced very high roll accelerations as a divergent Dutch roll type of maneuver developed. Roll rates were extremely high, ... This ma-*

neuver was disorienting, and I pulled back on the stick to increase the angle of attack, trying to damp it out. The first thing that entered my mind was that the interconnect was too high so, as soon as I was able to get hold of the situation, I checked my interconnect; it was 0.45, about where I wanted it. The corrective action of pulling back on the stick damped out the maneuver."

The pilot's comments illustrate PIOs are very alarming and disorienting to the human operator. The comments also show that the pilot is usually unaware he/she is actually contributing to the oscillation. Instead, the pilot generally thinks the vehicle dynamics have changed due to some sort of control system malfunction or mechanical failure. In this case, the pilot thought the interconnect ratio (which is a control system gain) had been inadvertently increased - though it had actually remained *unchanged.*

The changes in vehicle attitude which are typical of a PIO can be seen in Figure 1-1. As the vehicle rolls out of the turn from -30 degrees bank angle (ϕ) at time zero, the pilot attempts to capture "wings level" (ϕ=0) by initiating negative aileron input (δ_{LS}) at 2 seconds. However, the vehicle rolls through zero bank angle slightly and then reverses direction. The pilot responds with opposite aileron control at around 5 seconds. At 7 seconds, the bank angle and roll rate (p) are seen to be diverging. Recovery is made, 11 seconds later, after three very large amplitude oscillations.

The pilots aileron control is seen to be approximately 180 degrees out of phase with the bank angle he is attempting to control. Reference [7] states, "since a PIO is evidence of an undamped closed-loop, pilot-vehicle oscillation, then there must exist at least one measurable aircraft state that is 180 degrees out of phase with at least one pilot control." An essential ingredient of a PIO is the phase lag of the pilot input with respect to the aircraft state he/she is trying to control. Most PIO prediction criteria endeavor to account for this important feature in some manner.

Reference [6] states the actual maximum bank angles reached by the M2-F2 were at least +90 and -120 degrees. These values had to be obtained from photographic coverage since the flight instrumentation was not considered accurate at bank angles in excess of 45 degrees. The roll rate is seen to be in excess of 60 degrees per second. The pilot aileron

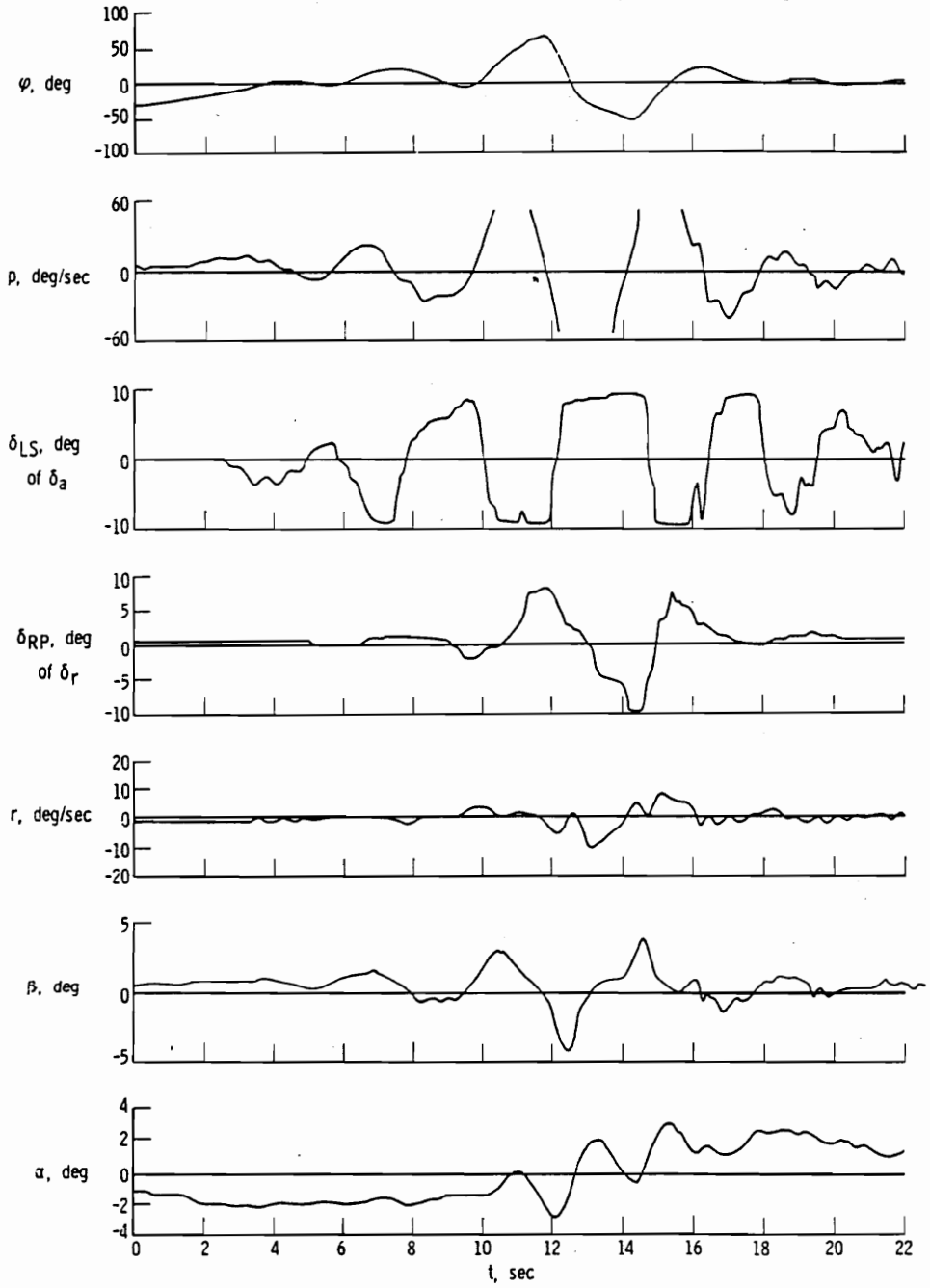

(a) Pilot's input and vehicle response.

Figure 1-1. Time Histories of M2-F2 PIO [6].

and rudder (δ_{RP}) inputs are seen to move rapidly from their maximum to their minimum values as the pilot tries to control the oscillation. The pilot is unaware that his dynamics are contributing to the oscillation. That is, the oscillation would subside if the pilot either released the controls or held them fixed. The oscillation damps out as the pilot manages to increase the angle of attack (α).

It is of little surprise that the pilot would find these rapid large amplitude oscillations "disorienting." Furthermore, since these oscillations begin "suddenly" with "no warning at all," it is understandable that a pilot would assume that some sort of malfunction had occurred that caused the vehicle dynamics to change instantly. In the case of the M2-F2, the PIO was attributed to a lightly damped coupled roll-spiral mode that appears at low angles of attack [6]. Since the damping of this coupled mode increases as the angle of attack is increased, the pilot was able to recover from the oscillation by pulling back on the stick thereby increasing the angle of attack

Another well known, or *famous*, PIO incident is the "unintentional" first flight of the General Dynamics YF-16 in 1974. A high speed taxi test resulted in a PIO of approximately 15 seconds in duration. During the event, roll rates in excess of 50 degrees per second were commanded, resulting in rate and position limiting of the control surface actuators [3]. In order to recover from the PIO, the pilot added power and began to climb resulting in the unintended first flight. As the vehicle began to climb, the PIO was successfully eliminated. The vehicle was able to circle the runway and land safely. In this case, the PIO was attributed to high pilot gain and control system lag at the high input frequencies [3].

The PIO encountered during the fifth flight of the "Approach and Landing Tests" (ALT-5) of the Space Shuttle Orbiter in 1977 is significant because the extensive coverage of the event focused attention on the phenomenon of PIO [5]. The landing was to be made at Edwards Air Force Base on a 15,000 ft runway. The touchdown point was approximately 5,000 ft beyond the runway threshold. A large crowd of spectators and newspeople had gathered near the touchdown point.

When the pilot decided he was going to land past the touchdown point, he attempted to "spike it on" [3]. A PIO started in pitch seven seconds prior to first touchdown, with a lateral PIO starting two seconds later. A more severe lateral PIO was observed after the first touchdown and bounce. The elevons were shown to be almost continuously rate limited as the Orbiter proceeded to skip and hop in a dramatic fashion until the pilot was finally able to gain control. The PIO, in this case, was attributed to excessive effective time lag that was aggravated by rate limiting effects [3].

Just as the high profile nature of the Space Shuttle ALT-5 incident peaked interest in the study of PIOs, recent accidents involving the JAS 39 Gripen in 1989 and 1993 and the Lockheed/Boeing YF-22A in 1992 have dramatically renewed interest in the investigation of this problem. With the increasing complexity of the modern aircraft comes an increasing potential of PIO due to the interaction of several dynamic factors. For example, consider the crash of the YF-22A. According to Reference [8], the landing gear of the aircraft were retracted at nearly the same time as the afterburner was ignited to initiate a planned go-around. These configuration changes caused significant mode switching in the aircraft control laws. The control law changes are usually governed by "transient-free" switches that slow the transition of control system gains from landing to up-and-away configuration. The pilot, on the other hand, must adapt his control strategy continuously and at the same rate as the aircraft dynamics are changing. Therefore, the PIO of the YF-22A is an example of several different dynamic elements contributing to the oscillation. Since the YF-22A prototype was highly instrumented and the PIO event was captured on film, it was possible to deduce the various dynamic interactions that ultimately lead to the crash.

The question is, however, could any of the existing PIO analysis methods have predicted the YF-22A PIO *before* it occurred? Most existing PIO analysis methods and criteria were developed to address individual dynamic effects. For example, it is usually assumed that the pilot is only controlling a single axis or moving only one manipulator. Most criteria cannot handle nonlinearities and few, if any, can address the combined effect

of several dynamic factors as in the YF-22A crash. Consequently, it is unlikely that an existing analysis method could have predicted the YF-22A PIO incident.

The problem of an undesirable coupling between the pilot and aircraft has been pervasive throughout the history of manned flight. The results of a PIO can be at best annoying and at worst catastrophic, leading to loss of both pilot and aircraft. Although the problem of predicting under what circumstances a PIO is likely to occur is by no means a new one, it has become more complicated as the dynamics of the aircraft and control system have become more complex.

1.1 Problem Definition

The two basic problems that need to be considered when studying PIO can be stated as follows:

1. ***PIO Prediction***: *Given a mathematical representation of a piloted vehicle, under what conditions, if any, is a PIO likely to occur.*

2. ***PIO Prevention:*** *The avoidance of the dynamic interactions that are suspected causes of PIO through the design of the aircraft and/or the control system.*

These two problems are closely related. In solving the first problem, insight is generally gained that assists in the solution of the second problem. Furthermore, within the scope of the PIO prediction problem, the underlying desire is to be able to differentiate between those aircraft that are prone to PIO and those aircraft that are resistant to PIO.

1.1.1 Definition of a PIO

The military flying qualities specifications [2] define a PIO as,

"a sustained or uncontrollable oscillation resulting from the efforts of the pilot to control the aircraft"

However, much discussion has been and probably will continue to be fervently pursued on a more precise definition of PIO. Such discussions include whether the pilot drives the

oscillation or the oscillation drives the pilot. Indeed, the very term "pilot-induced oscillation" has been challenged by several researchers with claims that the term places undue blame for the event on the pilot. It has been suggested that the term be replaced by "pilot-in-the-loop oscillation" which removes the emphasis that the pilot induces the oscillation but has the benefit of retaining the PIO acronym. A'Harrah [9 and 10] goes a step further in suggesting that the term "aircraft-pilot coupling" (A-PC) should be used noting that it is an aircraft deficiency that is the root cause of the problem. While the assertion that the problem is indeed an aircraft deficiency is correct, the term PIO is certainly recognized by all those who work in the design and flight testing of high performance military as well as civil transportation aircraft and therefore will be used throughout this thesis.

Arguments also continue regarding whether certain oscillation events are PIOs. For example, oscillations can occur during air-to-air refueling. However, if we proceed from the standpoint that a PIO prone aircraft is undesirable, then any PIO behavior is inherently unacceptable. If there are oscillation tendencies due to coupling of the aircraft and pilot which have relatively benign characteristics, then these should be dealt with as separate handling qualities issues. The term PIO should be reserved for description of an unacceptable coupling between the pilot and aircraft so that it keeps its current day connotations and continues to be cause for the greatest concern.

It is not the purpose of this thesis to argue the semantics of the terminology associated with PIO. Therefore, for the purposes of this study, the following definition is employed,

> ***A PIO results when the closed-loop, pilot/vehicle system oscillates due to a loss in asymptotic stability.***

Since the analysis methods to be presented here deal primarily with mathematical models of the pilot and aircraft, this definition is readily tested. Asymptotic stability of a linear system is lost when any pole (or complex pair of poles) move from the left half plane onto the imaginary axis. For a nonlinear system, in addition to examining the poles of the corresponding linearized system, the existence of a limit cycle (sustained oscillation) will be

taken as a separate measure that precludes the condition of asymptotic stability of the closed-loop system.

In his definition of A-PC, A'Harrah includes the case of pilot/vehicle divergence. Divergence is a non-oscillatory response in which control inputs and control surfaces are generally locked at maximum deflection. However, in this case, the pilot/vehicle system is no longer behaving in a closed-loop manner and as such will not be considered in the current analysis.

1.1.2 Causes of PIO

Several dynamic factors have been documented as contributing to the occurrence of PIO [5]. These can be separated into those that are attributed to the linear dynamics of the aircraft and pilot, and those that are nonlinear in nature. Also, it has been noted by several researchers that a trigger event is often necessary to excite the PIO. A brief list of the causes of PIO and a description of events associated as triggers is given below.

Linear

Aspects of the linear dynamics of an aircraft that have been associated with causing PIO include:

- sluggish response modes
- lightly damped modes
- low stick force per g
- sensitive stick gradients
- unusual coupling responses
- excessive time lags in the augmented aircraft

Nonlinear

Nonlinearities associated with PIO include:

- surface actuator rate and position limiting
- nonlinear stick characteristics
- mode switching

Trigger Events

While trigger events are not causes of PIO *per se*, they are often needed to excite a response of the pilot that will "trigger" or start the oscillation event. A trigger event can be something as simple as a gust of wind or something more complicated such as control system mode switching, a control system failure, or an aircraft structural failure. In the subsequent analysis, closed-loop stability is analyzed in the face of changes in both the aircraft and pilot models. In other words, some trigger event has caused the pilot and/or aircraft dynamics to change. That is, the post trigger dynamic situation is to be analyzed.

1.1.3 PIO Classifications

Given that there are several distinct and diverse causes of PIO, it is desirable to group the oscillation events in some useful manner. To this end, McRuer [5] has proposed classifying PIOs according to three separate categories. The proposed categories yield a convenient mechanism with which to discuss the current research and are repeated in Figure 1-2.

In short, Category I PIOs can generally be described by linear dynamics associated with coupling of the pilot and vehicle. Category II PIOs allow the introduction of actuator rate and/or position limiting as the dominating nonlinearities. Category III PIOs are by far the most complicated, allowing completely nonlinear pilot and vehicle dynamics that can be in transition during the oscillation. The above categories are intended to differentiate PIOs on the basis of current modeling and analysis techniques and not on the severity of the resulting oscillations. As a matter of interest, it should be noted that severe PIOs can occur within each of the categories.

Category I - Essentially Linear Pilot-Vehicle System Oscillations: The effective controlled element characteristics are essentially linear, and the pilot behavior is also quasi-linear and time-stationary. The oscillations are associated with high open-loop system gain. The pilot dynamic behavior mode may be pursuit, compensatory, precognitive, or synchronous.

Category II - Quasi-Linear Pilot-Vehicle System Oscillations with Surface Rate or Position Limiting: These are severe PIOs, with oscillation amplitudes well into the range where actuator rate and/or position limiting in series with the pilot are present as primary nonlinearities. The rate-limited actuator modifies the Category I situation by adding an amplitude-dependent lag and by setting the limit cycle magnitude. Other simple nonlinearities (e.g. stick command shaping, some aerodynamic characteristics) may also be present. These are the most common true limit-cycle severe PIOs.

Category III - Essentially Non-Linear Pilot-Vehicle System Oscillations with Transitions: These PIOs fundamentally depend on nonlinear transitions in either the effective controlled element dynamics, or in the pilot's behavioral dynamics. The shifts in controlled element dynamics may be associated with the size of the pilot's output, or may be due to internal changes in either control system or aerodynamic/propulsion configurations, mode changes, etc. Pilot transitions may be shifts in dynamic behavioral properties (e.g. from compensatory to synchronous), from modifications in cues (e.g. from attitude to load factor), or from behavioral adjustments to accommodate task modifications.

Figure 1-2. Proposed PIO Classifications from Reference [5].

1.2 Objective

Several useful PIO criteria currently exist. However, these criteria (almost exclusively) directly address only the Category I PIO situation. It is the belief of many researchers that the existing methods adequately predict Category I PIO susceptibility. A few have even gone as far as to say PIOs could be eliminated by simply meeting Level 1 Flying Qualities specifications. Therefore, it is the purpose of this research to begin to deal, in a direct and structured manner, with the more complicated Category II and Category III PIOs. In this vein, the current research is not meant to replace the valuable work that has preceded and inspired it, but to augment that work instead.

An analysis method is sought which is capable of handling the combined effects of all influencing dynamic elements in a structured fashion. The analysis method should be capable of handling any combination of the suspected causes of PIO as described in Section

1.1.2. The underlying motivation is to distinguish between PIO prone and PIO resistant aircraft. Again, the application of this analysis should yield enough insight into the PIO problem to suggest design methods to aid in the avoidance of the dynamic interactions responsible for causing PIOs.

1.3 Approach

This research deals primarily with computational analysis techniques designed to predict PIO susceptibility of modern aircraft. These techniques are intended for use during aircraft development or modification prior to flight. Methods to study PIO behavior during flight test and manned simulations will not be discussed. Aircraft and pilot modeling will only be addressed to the extent required to utilize the PIO analysis methods.

The basic premise of this research can be stated as follows:

> ***A PIO resistant aircraft resists closed-loop pilot dynamic variations in the face of nonlinear aircraft behavior.***

That is, if the closed loop pilot/vehicle system remains stable for assumed variations in the pilot and aircraft models, the aircraft will be deemed resistant to PIO. It could be argued that nonlinear aircraft behavior causes the pilot to change his/her equalization instead of vice versa. From an analysis point-of-view, the simultaneous action of the aircraft and pilot dynamics can represent either situation.

The basic premise of this research involves the study of pilot/aircraft stability robustness and nonlinear system oscillations. Therefore, the proposed analysis method is a combination of multivariable stability robustness analysis and multivariable describing function analysis. These methods were developed specifically to handle multiple dynamic effects simultaneously.

This research effort is comprised of several tasks. The first task consists of the development of the necessary stability analysis software. Existing computational analysis algorithms have been collected and refined. The MATLAB™ computer-aided engineering software package is used as the computational environment in which all analysis is con-

ducted. Since other competing packages have similar programming (or macro) features, it is expected that translation to other packages can be easily completed.

The four basic computational tasks that must be carried out are:

1) Compute the pilot model
2) Construct the unified block diagram
3) Perform a structured singular value analysis
4) Search for limit cycles

Algorithms already exist (in MATLAB™ form) to compute "optimal control" models of the human pilot [11 and 12], and no modification is necessary for use in the current PIO analysis. SIMULINK™, an optional program linked to MATLAB™, is used to perform the necessary block diagram manipulations and simulations. SIMULINK™ is an excellent environment for study of systems with simple isolated nonlinearities of the type generally used in PIO investigations. The algorithms to perform the real structured singular value analysis and the limit cycle search were also coded within the computational framework of MATLAB™. The algorithms are based on those currently available in the open literature.

The second task was to perform software validation studies. Once all of the analysis codes have been implemented and tested, case studies are conducted using existing aircraft data. The stability robustness software is exercised utilizing configurations in the database of Reference [13]. This database, which was developed to study PIO, has been referred to elsewhere [14] as the HAVE PIO database, and that designation is continued here. The multivariable limit cycle software is then separately validated using a previous study of back-up control system designs for the F-4 aircraft [15]. The original study was intended to show the PIO susceptibility of the back-up control systems. This application is particularly appealing because both control surface rate and deflection limiting were shown to occur simultaneously.

Finally, the desire is to illustrate the capabilities of the new analysis method as applied to a somewhat complicated nonlinear pilot/vehicle system. To this end, the M2-F2 lifting body is used to study the effect of combinations of nonlinear dynamic elements. The M2-

application illustrates how the unified PIO analysis method can be used to isolate combinations of dynamic elements that can lead to oscillatory behavior.

1.4 Organization

Chapter 2 contains a review of the existing PIO literature. The purpose of this review is to highlight the various approaches and show how they form a foundation for the new, unified, PIO analysis method.

The unified PIO analysis method process is then detailed in Chapter 3. Here the analysis technique is stated as a well structured five step process. The technical details of the application of the analysis technique are given. Where appropriate, the supporting mathematical algorithms and verification studies are also presented.

An example of the PIO analysis procedure as applied to the M2-F2 is given in Chapter 4. The five step process is carried out in detail and the results analyzed as to their relation to the PIO characteristics of the vehicle. These results are compared to those available in the literature. The final chapter contains a summary of the conclusions that can be drawn from this research effort and some suggestions for further work in this area.

2 Review of Existing PIO Criteria and Methods

As with all research, the current effort is intended to build on the base of knowledge and experience that has proceeded it. This chapter presents a review of some of the published research dealing with the analysis and prediction of pilot-induced oscillations.

The research conducted by Hirsch and McCormick [16] is representative of the early study efforts into the nature of pilot-induced oscillations. Fixed and moving base simulations were used to experimentally determine pilot dynamics. PIOs were induced by altering the longitudinal dynamics of the aircraft. The analysis consisted of experimental observations and simple root locus plots that assumed the pilot dynamics could be represented as a pure gain. This work not only showed the importance of including simple pilot compensation strategies, but also revealed the importance of considering both visual and motion cues in the analysis.

Most existing PIO analysis methods are, in some way, based on the data collected by Neal and Smith [17]. In the early 1970s, Neal and Smith conducted flight test experiments investigating the effects of control system dynamics on the longitudinal flying qualities of fighter aircraft. They developed a criteria based on the assumption of closed-loop attitude control during tight tracking. A lead/lag model of the pilot was incorporated in the analysis. The form of this model is given as,

$$Y_p = K_p\left(\frac{T_1 s + 1}{T_2 s + 1}\right)e^{-\tau_d s} \tag{2-1}$$

The model consists of a variable gain (K_p), a variable first order compensation network (T_1 and T_2), and a pilot time delay that is assumed constant ($\tau_d \approx 0.3$ sec).

In the analysis procedure, the pilot model parameters are adjusted to minimize the peak resonance of the closed-loop frequency response magnitude subject to attaining a specified bandwidth. A constraint is placed on the minimum magnitude at low frequencies.

Figure 2-1 shows the parameter regions that define the Neal-Smith criteria. The parameters of the criteria are the resonant peak magnitude ($|\theta/\theta_c|_{max}$) and the phase angle of the pilot compensation ($\angle$pc) at the bandwidth frequency. Handling qualities ratings are penalized as the pilot model is required to generate lead or lag compensation in order to meet the desired bandwidth. Furthermore, if it is not possible to reduce the peak magnitude sufficiently, then handling qualities ratings suffer and a strong PIO tendency is predicted. The Neal-Smith criteria emphasize the shape of the closed loop frequency response and illustrate a successful application of pilot modeling techniques to understanding and predicting the pilot/vehicle interaction.

One of the most widely recognized and applied PIO analysis methods is that developed by R. Smith [18]. In its initial development, Smith made use of McRuer's crossover pilot model [19] to describe the dynamic interaction between the pilot and the vehicle. However, as the criteria evolved to become the Smith-Geddes criteria [20], only the vehicle attitude-to-stick force transfer function was utilized. The Smith-Geddes criteria, which is often referred to as the R. Smith criteria, involves defining a criterion frequency that is derived from the magnitude slope of the vehicle frequency response between 1 and 6 rad/sec. The criterion frequency is given by,

$$\omega_{cr} = 6.0 + 0.24S \quad \text{(rad/sec)} \tag{2-2}$$

where S is the computed magnitude slope in dB/octave.

The phase angle is checked at the criterion frequency. If the phase angle is found to be less than -180 degrees at the criterion frequency, then the aircraft is predicted to be prone to PIO. If the phase angle is found to be between -165 and -180 degrees at the criterion frequency, then the aircraft is predicted to be PIO sensitive. The aircraft is predicted PIO resistant if the phase angle is greater than -165 degrees. Furthermore, the criterion frequency is taken as the predicted PIO oscillation frequency.

Consider application of the Smith-Geddes criteria to two configurations of the HAVE PIO database [13]. Figure 2-2 shows the Bode diagram for configurations H2-1 and H2-5. The average PIO rating for Configuration H2-1 was 1.0. Configuration H2-5 was

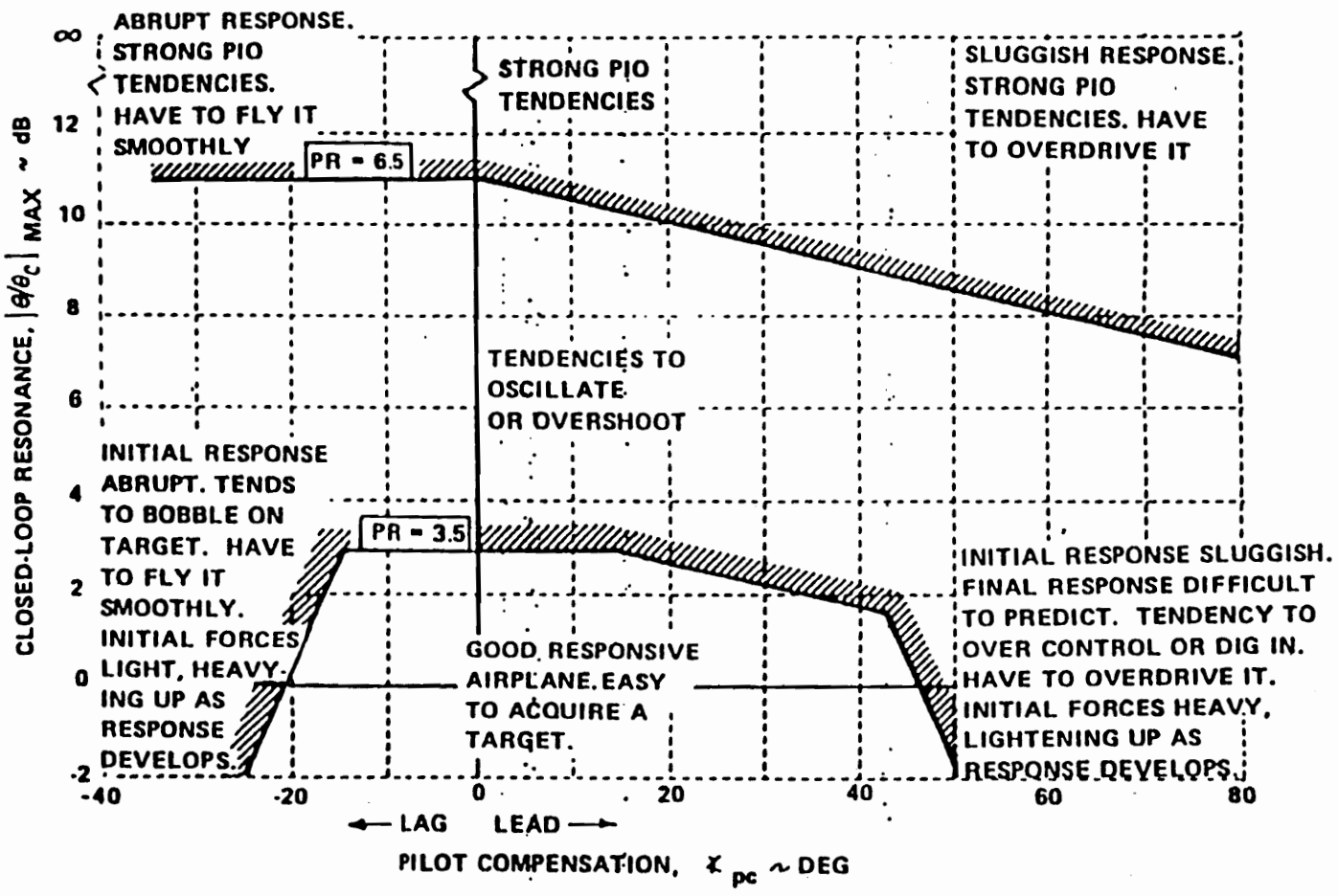

Figure 2-1. Neal-Smith Criterion [17].

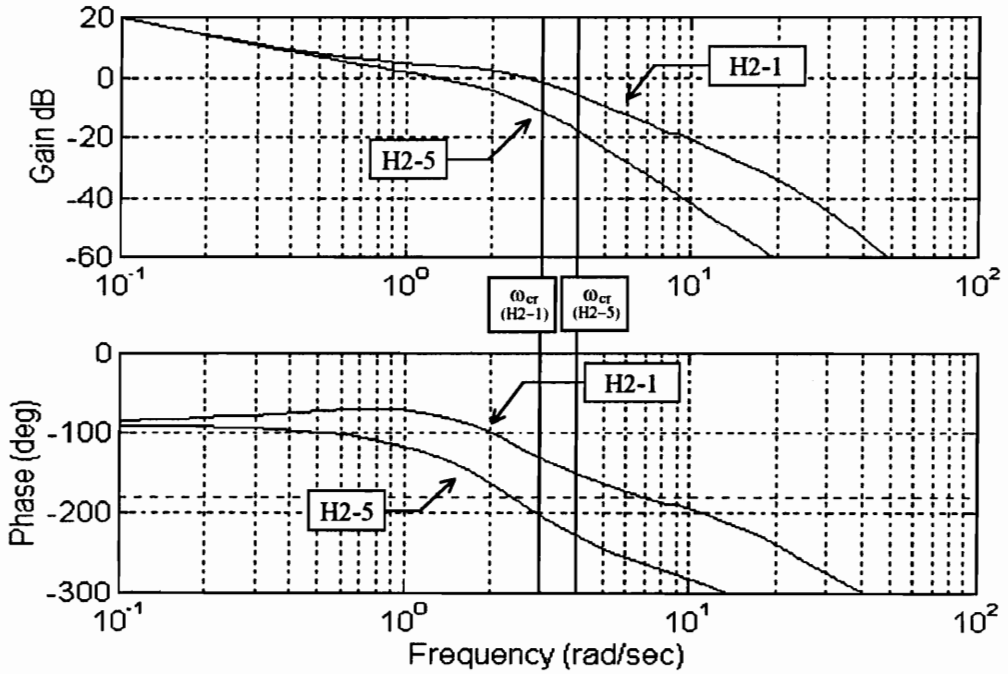

Figure 2-2. Bode Plots for HAVE PIO Configurations H2-1 and H2-5.

given an average rating of 4.4. An aircraft receiving a PIO rating above 2.0 is considered susceptible to PIO. Therefore, configuration H2-1 was evaluated to be PIO resistant while Configuration H2-5 was found to be PIO prone.

A large negative amplitude slope reduces the criterion frequency. Since the aircraft transfer function phase angle generally becomes more negative at higher frequency, a reduction in criterion frequency naturally leads to a larger phase angle. Therefore, the Smith-Geddes PIO criterion tends to identify aircraft configurations having the characteristic of large negative magnitude slopes in the frequency range of 1.0 to 6.0 rad/s as PIO resistant. Since the Smith-Geddes Criterion phase angle is -180 deg, it is reasonable to suggest that configurations with larger phase crossover frequencies (the frequency where the phase angle is -180 deg) will be predicted PIO resistant. In addition, an aircraft with a shallow phase angle slope in the same frequency range will decrease the phase angle sensitivity to criterion frequency changes and will likewise be predicted less PIO prone.

In the frequency range from 1.0 to 6.0 rad/sec, Configuration H2-5 has a steeper magnitude slope than Configuration H2-1, but H2-1 exhibits a shallower phase angle slope and a larger phase crossover frequency. Although the criterion frequency for H2-5 is lower than that for H2-1 (approximately 3 rad/sec as opposed to 4 rad/sec), the phase angle for H2-5 is less than -180 deg and the phase angle for H2-1 is greater than -165 deg at their corresponding criterion frequencies. Based on the Bode plots of Figure 2-2, application of the Smith-Geddes criteria predicts Configuration H2-5 to be more susceptible to PIO than Configuration H2-1.

Mitchell and Hoh advocate a PIO criterion that specifies the maximum phase angle change after the phase angle crosses -180 degrees [7]. The criterion is specified in terms of a phase delay parameter (τ_p) that is defined by,

$$\tau_p = \frac{\Delta\Phi}{2(57.3)\omega_{180}} \tag{2-3}$$

where $\Delta\Phi$ is the phase loss from ω_{180} to $2\omega_{180}$ and ω_{180} is the phase crossover frequency. An aircraft is considered susceptible to PIO if the phase delay (τ_p) is greater than or equal to .12 sec (.15 sec in landing).

Small values of the phase delay parameter are required to label an aircraft PIO resistant using this criterion. Therefore, this criterion will predict as PIO resistant those configurations with higher phase crossover frequencies and shallower phase angle slopes after phase crossover. The phase delay parameters for the two HAVE PIO configurations can be calculated from Figure 2-2. The phase delay parameters are found to be 0.04 and 0.24 for configurations H2-1 and H2-5 respectively. Again, Configuration H2-5 is seen to be more prone to PIO than Configuration H2-1.

One of the most prolific researchers in the area of PIO investigation has been R.A. Hess [14, 21, and 22]. Dr. Hess has used much more complex and intricate models of the human operator in an effort to more accurately represent the interaction between the pilot and the aircraft. Hess's 1991 paper, Reference [14], develops a PIO prediction method that limits the bandwidth and slope of the pilot/vehicle open-loop transfer function. The

Hess-Kalteis Criterion is shown in Figure 2-3. The boundary limits the minimum gain crossover frequency to 2.0 rad/sec. Furthermore, for a pilot/vehicle open-loop frequency response with a gain crossover frequency of exactly 2.0 rad/sec, the criterion limits the magnitude slope to at least -20 dB/decade in the neighborhood of the gain crossover frequency. Thus, the criterion tends to identify configurations with steeper magnitude slopes in the gain crossover frequency range as PIO resistant.

The success of Hess's method relies heavily on an accurate model of the human pilot. In his PIO studies, Hess uses the Optimal Control Model (OCM) of the human operator. This model was developed by Kleinman, Baron, and Levison in 1970 [23]. It has also been used by other researchers to develop PIO criteria for different aircraft types and flight tasks [24-26]. These researchers have developed criteria using frequency-domain representations of either the open- or closed-loop pilot/vehicle transfer function. Closed-loop resonant peaking behavior (References [25] and [26]) and open-loop crossover properties (References [22] and [24]) have been effective PIO predictors.

These PIO analysis methods share common features. The Neal-Smith and Hess-Kalteis criteria incorporate pilot models to capture the dynamic interaction between the pilot and the aircraft. The Neal-Smith criterion examines the magnitude peak resonance of

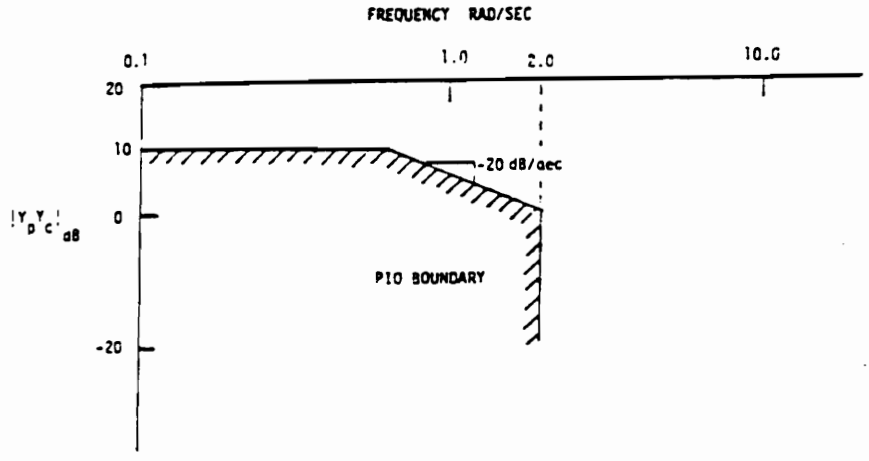

Figure 2-3. Hess-Kalteis PIO Criterion [14].

the closed-loop pilot/vehicle transfer function. The Hess-Kalteis criterion examines the open-loop pilot/vehicle transfer function and favors a large negative amplitude slope to label an aircraft PIO resistant.

The Smith-Geddes and phase delay criterion are based on examination of the open-loop aircraft transfer function. These two criteria favor large values of the phase crossover frequency and shallow phase angle slope to label an aircraft PIO resistant. Like the Hess-Kalteis criterion, the Smith-Geddes criterion favors a large negative amplitude slope to label an aircraft resistant to PIO.

In particular, these criteria deal directly with the shape of the aircraft or pilot/aircraft transfer function near where the phase angle is -180 degrees and near where the pilot/vehicle crossover frequency is likely to occur (1-6 rad/sec). Recall that the goal of these criteria is to distinguish those aircraft with PIO tendencies from those resistant to PIO. That is, the criteria attempt to determine which aircraft configurations have tendencies to lose stability under closed-loop pilot control. Furthermore, Anderson shows how some of these analysis methods can be motivated by how arbitrary pilot dynamic changes can affect closed-loop stability [27]. Therefore, these methods would appear to relate directly to stability robustness with respect to variations in the pilot dynamics.

The phase crossover, or *neutral stability*, frequency is a critical feature in stability analysis. Recall the importance of the phase relationship between the pilot input and the vehicle response from the M2-F2 PIO example of Figure 1-1. The stability boundary of the closed-loop pilot/vehicle system is sought in PIO analysis. The thesis approach in Section 1.3 requires a combination of pilot modeling and stability robustness analysis to examine the effect of dynamic variations on closed-loop stability.

The existing criteria are deficient in handling the significant nonlinearities present in the close-loop pilot/vehicle system. The existing criteria directly address only the Category I PIO situation. Graham and McRuer have noted certain PIOs are analogous to the limit cycle behavior exhibited in some nonlinear systems [28]. In recent studies, R. Smith [29] has been using a nonlinear contactor model of the human pilot and searching for limit

cycles as a method of predicting fully developed PIO behavior. However, with the exception of Reference [15], little work has been completed to deal with several dynamic variations simultaneously. In order to address the nonlinear Category II and Category III PIOs, a multivariable describing function technique is considered in the technical approach. The technique is used to determine under what conditions the nonlinear pilot/vehicle system is capable of a producing a self-sustaining oscillation (limit cycle).

3 PIO Analysis Process

The analysis process outlined in this chapter is intended to distinguish between aircraft that are PIO prone and aircraft that are PIO resistant. The investigation is based on determining the stability of the closed-loop pilot/aircraft system in the face of variations in the pilot model as well as uncertainties in key aircraft parameters. The process is able to account for many of the nonlinearities in both the pilot and aircraft that are known contributors to PIO behavior.

3.1 Process Outline

Because PIO is characterized by a sustained oscillation, the underlying purpose of the analysis is to determine under what conditions the pilot/aircraft system is capable of producing such an oscillation. The unified multivariable analysis method consists of five steps. The first step is to determine an analytical model of the human pilot that is appropriate for the flying task under study. Any accepted modeling method can be used, although the resulting criteria may vary. Both crossover and "optimal control" model forms are acceptable. A synchronous (constant gain) model is also appropriate for some cases although a model with at least a -20 dB/decade high-frequency roll-off characteristic (to help attenuate feedback signal superharmonics) is desirable. Nonlinear pilot models, such as Smith's contactor model, can also be used.

The second analysis step is to identify and isolate the dynamic elements suspected of contributing to PIO behavior. Linear and nonlinear elements can be considered simultaneously. As mentioned previously, aerodynamic nonlinearities, control system nonlinearities, nonlinear stick gradients, various pilot model parameters, and control surface rate limits are of particular interest.

The third step is construction of a unified analysis diagram. The analysis diagram isolates those dynamic elements suspected of contributing to PIO. Only a single diagram need be constructed for the subsequent stability analysis. From this single diagram, the

stability of the closed loop pilot/vehicle system can be analyzed with respect to any combination of dynamic variations suspected of contributing to PIO.

The fourth step is to perform a stability robustness analysis using the structured singular value method. This analysis will yield a bound on the largest allowable parameter variation before instability is possible. The structured singular value analysis leads to a sufficient condition for stability and may be conservative. However, if the closed-loop system operates in a fashion such that the predicted bound on the uncertainty is not exceeded, then the closed-loop system will remain stable and will *not* exhibit limit cycle behavior. If the predicted bound is exceeded, the system may or may not be unstable and may or may not exhibit limit cycle behavior.

The final analysis step is to search for limit cycle behavior of the nonlinear pilot/aircraft system. A limit cycle is a self-sustained oscillation that is particular to nonlinear systems. The limit cycle search is carried out in the frequency domain. Results yield frequency and amplitude of the oscillation as well as a prediction of limit cycle stability. In most cases, limit cycle predictions can be confirmed using nonlinear time domain simulations.

3.2 Pilot Modeling

Advances in the theory of pilot modeling have led to new theories of pilot-induced oscillations. A number of different pilot models are suitable for PIO analysis. Early PIO criteria involved concepts generated from the crossover model of the human operator while more recent research has focused on the optimal control model.

The crossover model, developed by McRuer [19], is based on the observation that the pilot adapts his/her dynamics such that the open-loop pilot/vehicle system can be approximated, in the neighborhood of the gain crossover frequency, by

$$Y_p Y_c \approx \frac{\omega_c e^{-\tau_e s}}{s} \tag{3-1}$$

where Y_p represents the pilot dynamics, Y_c represents the vehicle dynamics, ω_c is the gain crossover frequency, and τ_e represents the effective time delay due to both the vehicle and

pilot dynamics. Therefore, the characteristics of the crossover model for the pilot (Y_p) will be different for each set of aircraft dynamics (Y_c), but the open-loop pilot/vehicle dynamics will be essentially the same. However, the crossover frequency and effective time delay will depend on the specific application.

Kleinman's Optimal Control Model (OCM) of the human operator is based upon Linear, Quadratic, Gaussian (LQG) control theory. The model includes a set of state-feedback gains that are computed using a special quadratic cost function. The state-feedback control law is then augmented with a state estimator and a predictor. The purpose of the predictor is to model the human's ability to adapt to his/her inherent (reaction) time delay.

A modified version of the Kleinman model has been developed by Davidson and Schmidt [30]. The Modified Optimal Control Model (MOCM) replaces the pure time delay with a Pade' approximation. The Pade' approximation recommended by Davidson and Schmidt is given by a second order form,

$$e^{-\tau_d s} \cong \frac{1-\tau_d s/2+(\tau_d s)^2/8}{1+\tau_d s/2+(\tau_d s)^2/8} \tag{3-2}$$

where τ_d is the human pilot time delay. The principal advantage of the Pade' approximation is that its use allows for direct computation of a human operator transfer function. Whereas Kleinman's model yields only frequency response information of the human response, the Davidson model provides a finite-dimensional state-space representation and detailed information of dominant response modes. Therefore, the interaction between the pilot and aircraft can be more readily identified.

The most common optimal MOCM cost function is assumed to be given by,

$$J = \int_0^\infty \left[e^2(t) + \rho \dot{\delta}_c^2(t)\right] dt \tag{3-3}$$

where e(t) is a displayed error signal and $\delta_c(t)$ is the pilot manipulator command input. The control rate weighting ρ is chosen to achieve the desired neuromuscular time constant as described in Reference [23]. Note that the error rate is usually retained in the pilot's

assumed observation vector but is not necessarily weighted in the cost function (3-3). Pilot models that minimize other cost functions, such as the H_2 and H_∞ transfer function norms, have also been recently reported by Anderson [11].

Unlike many PIO criteria, the unified PIO analysis method can also handle nonlinear pilot models. For example, Smith has described a contactor pilot model for study of fully developed PIO behavior [29]. The contactor nonlinearity is a relay that yields a fixed positive value for any positive input and a fixed negative value of any negative input. For example, if the input to the nonlinearity is +1, the relay output might be +2. For an input of +4, the output of the same relay is still +2. This model essentially represents a pilot that is manipulating the control so that it is always against either the positive or negative control limit.

3.3 Identify Dynamic Elements Suspected of Contributing to PIO

With models of the aircraft dynamics and the human pilot defined, the elements suspected of contributing to PIO must be identified and isolated. The elements of the aircraft directly associated with the causes of PIO given in Section 1.1.2 should be considered here.

Since the pilot model plays a key role in the unified analysis, any of the pilot model parameters may need to be considered as uncertain elements that can contribute to PIO tendency. The underlying concept of the closed-loop analysis is that a PIO resistant aircraft will remain stable in the face of variations in the pilot model. At this point, certain aspects of the model seem reasonable to consider. The most obvious suspect is the pilot gain. Increased pilot gain is often associated with tight tracking tasks such as precision approach and landing. Elevated pilot gain can also result when a pilot becomes aggressive or excited. Variations in other pilot model parameters (such as pilot time delay or lead time constant) are also of interest in the study of PIO.

3.4 Construct Unified Analysis Diagram

Perhaps the most important contribution of the structured singular value method is the construction of analysis block diagrams like Figure 3-1. The transfer function matrix M(s) in Figure 3-1 does not necessarily represent the aircraft, the pilot, or a series combination of feedback loop elements. Instead, M(s) represents the transfer function matrix as seen by each model parameter that is considered varying – regardless of where the parameter occurs in the feedback loop. For example, a variation due to actuator rate limiting can be analyzed in conjunction with a variation in the pilot's loop gain. Consequently, model variations from many different sources can be analyzed simultaneously.

An essential part of the stability robustness analysis is the construction of the M(s) matrix shown in Figure 3-1. A first step involves identification of the uncertainties to be analyzed. Three basic representations of uncertainty, or parameter variation, will be considered herein. Figure 3-2 shows both a multiplicative and an additive uncertainty. The variation (δ) represents a percentage signal change for the multiplicative uncertainty and an absolute change for the additive uncertainty. Since many different uncertainties may be

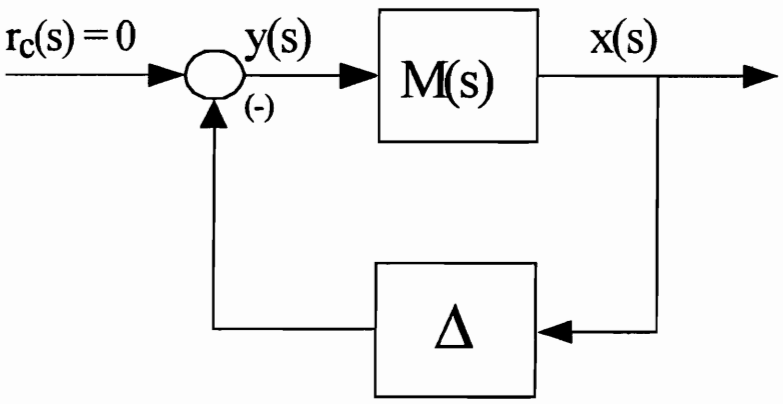

Figure 3-1. Unified Analysis Diagram.

included in the analysis, it will be convenient to scale these variations. Each variation is scaled by introducing a scaling gain (k) as shown in Figure 3-2.

Figure 3-3 illustrates the modeling of a nonlinear saturation by an equivalent, but variable gain. When the scaled variation (kδ) is zero, the equivalent gain is equal to the slope (L) of the linear portion of the saturation. In this case, the input to the saturation element

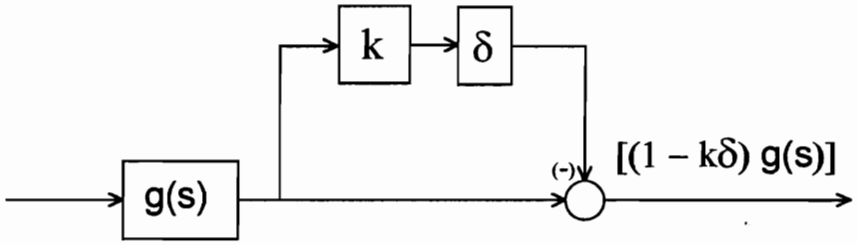

a) Multiplicative Uncertainty

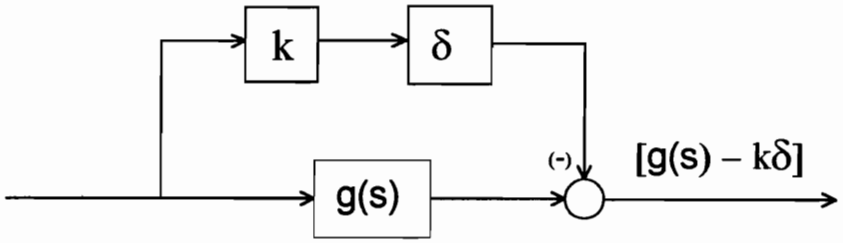

b) Additive Uncertainty

Figure 3-2. Representation of Uncertainty.

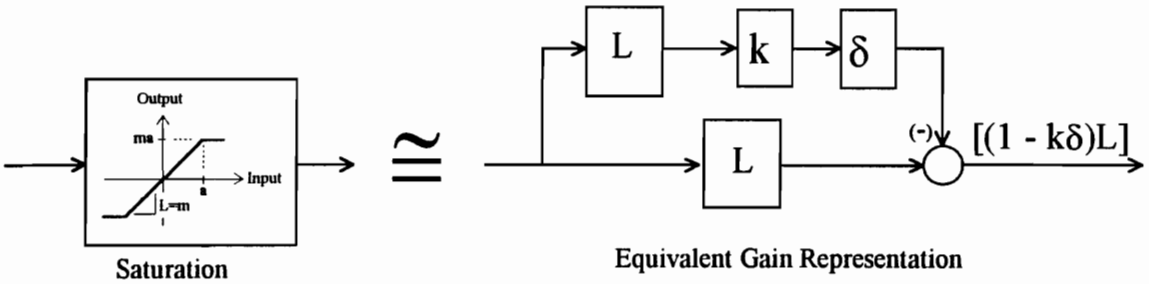

Saturation

Equivalent Gain Representation

Figure 3-3. Representation of a Nonlinear Saturation Element by an Equivalent but Uncertain Gain.

is less than the saturation limit and the element is not saturated. As the input to the element increases above the saturation limit, the effective gain is reduced. The reduction in the equivalent gain is accomplished by allowing $k\delta$ to vary from zero to +1. The element is completely saturated when $k\delta$ equals +1. That is, the output of the block diagram in Figure 3-3 is zero. Therefore, the effective gain is a function of the input to the saturation element with $k\delta$ being proportional to the percent saturation of the element.

Within the current framework, it is convenient to cast the multivariable describing function problem in a form similar to that required for stability robustness analysis. Using a standard M-Δ configuration to define the structure of the nonlinear system brings a needed organization to the general problem of predicting the occurrence of limit cycle behavior and allows the construction of a single, unified analysis diagram. In the describing function case, M(s) represents the transfer function matrix as seen by the nonlinear elements and as such can contain parts of the vehicle, control system, and pilot. Whereas each δ represents a bounded parameter variation in the stability robustness analysis, each δ will be replaced by a describing function representation of the nonlinear element during the search for limit cycle behavior. The analysis diagram is to set up such that the nominal system is obtained by setting all the individual δs to zero. Therefore, the effect of any combination of uncertainties can be found by allowing only the corresponding δs to vary.

Once the individual uncertainties have been selected for study, the system must be put in the M-Δ form for analysis. While some algorithms exist to aid in the construction of the necessary matrix [31], it is suggested that a graphical simulation program like SIMULINK™ be used to determine the state-space model for M(s). SIMULINK™ allows the user to isolate the input and output from any element in the loop and to then linearize the system. To linearize a system, SIMULINK™ *inport* and *outport* elements are placed around the uncertainties as illustrated in Figure 3-4. This diagram is for multiplicative uncertainty shown in Figure 3-2(a). Note that a negative sum is needed to generate M(s) that is consistent with Figure 3-1. With all the *inport/outport* pairs in place, a state-space model of M(s) is produced using the MATLAB™ *linmod* command. With M(s)

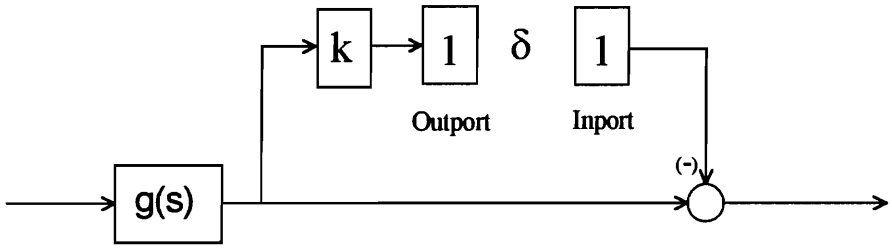

Figure 3-4. Model of Uncertainty in a SIMULINK™ Diagram.

computed, the effect of the modeled uncertainties on system stability is analyzed. Note that the system under study can be completely linear (and not need to be linearized *per se*). However, the *linmod* feature of MATLAB™ provides a convenient and useful way to form M(s) for complicated block diagrams.

Again, M(s) represents the dynamic system as seen by every parameter (δ) that is considered as an uncertainty (or variation) that may lead to undesired closed-loop pilot/vehicle oscillations. Since the nominal system is obtained by setting all δs equal to zero, M(s) need only be found a single time. Any particular combination of parameter variations can then be considered in either the stability robustness or the describing function analysis by considering the proper elements (rows and columns) of the M(s) matrix.

3.5 Stability Robustness Analysis

A PIO is fundamentally a stability problem. Sustained oscillations only occur in linear systems when the dynamics of the system lose damping. An example is an undamped spring-mass system that will oscillate from an initial displacement with constant amplitude motion.

Stability robustness analysis is the study of how model parameter variation or "uncertainty" affects feedback loop stability. Since the mid 1980's, a resurgence in frequency-domain analysis methods for stability robustness has occurred. These methods have relied on the singular value matrix norm as a "measure" of relative stability. For example, gain and phase margins for multivariable feedback systems can be defined using the

singular-value based analysis method [32]. Stability margins defined in such a manner are very useful in that they define the gain or phase variation that can occur *simultaneously in each feedback loop.* As a result, an investigation of multiple parameter variations can be carried out rather easily.

Doyle is widely regarded as the key developer of the structured singular value analysis method [33]. The structured singular value method allows the research engineer to investigate not only simultaneous model parameter variations, but also the effect of multiple parameters located arbitrarily throughout the feedback system. Thus, parameter variation is not confined to just the feedback loop signals, but can include individual system parameters.

3.5.1 Basic Theory

Stability of the feedback loop can be investigated from the loop equations represented in Figure 3-1,

$$y(s) = -\Delta\, x(s) \tag{3-5}$$

$$x(s) = M(s)\, y(s) \tag{3-6}$$

Solving (3-6) in terms of x(s) yields,

$$[I + M(s)\Delta]\, x(s) = 0 \tag{3-7}$$

The matrix $[I + M(s)\Delta]$ is known as the return difference matrix. Stability robustness analysis involves finding the size of the (block) diagonal matrix Δ that satisfies $\det[I + M(j\omega)\Delta] = 0$. Doyle, therefore, defined the structured singular value $\mu(M,\omega)$ as,

$$\frac{1}{\mu(M,\omega)} = \min_{\Delta} \{\sigma_{max}(\Delta) \mid \det[I + M(j\omega)\Delta] = 0\} \tag{3-8}$$

where σ_{max} is the largest matrix singular value.

The structured singular value computation attempts to find the smallest uncertainty block Δ that can destabilize the feedback system. Since the minimization problem of Equation (3-8) can be difficult to solve, Doyle derived expressions for upper and lower bounds on the structured singular value. Namely,

$$\max_{U} \rho(UM) \leq \mu(M,\omega) \leq \min_{D} \sigma_{max}(DMD^{-1}) \qquad (3\text{-}9)$$

where U is unitary and D is a real scaling matrix such that $D\Delta D^{-1} = \Delta$. The lower bound is not generally used as a measure of robustness but is used to determine how close the upper bound approximates the exact value.

For most practical systems, the upper and lower bounds differ by less than 15%, showing the upper bound to be a reasonable approximation [34]. The upper bound is still posed as an optimization problem, but it is one that has no non-global minima [35]. This optimization involves finding the scaling matrix that minimizes the maximum singular value of DMD^{-1}. The optimum scaling matrix D can be found through standard nonlinear optimization techniques, but is often approximated using an iterative method first developed by Osborne [36]. Osborne's technique finds that D which minimizes the Frobenius norm of DMD^{-1}. Because the Frobenius norm acts as an upper bound on the 2-norm (maximum singular value), reducing the Frobenius norm helps reduce the 2-norm [35]. Since the Frobenius norm is an upper bound on the 2-norm, use of Osborne's technique to select D yields a conservative estimate of the stability margin, but the technique is very efficient.

As given above, the elements of Δ can be complex. When the parameter variations modeled in Δ are known to be real only, a less conservative upper bound, reported by Jones [34], can be found for the structured singular value. This upper bound is given by,

$$\mu_r(M,\omega) \leq \min_{D} \{ \max_{\Phi} \sigma_{max}[(DM(j\omega)D^{-1}\Phi + (DM(j\omega)D^{-1}\Phi)^T)/2]\} \qquad (3\text{-}10)$$

where D is determined as before. The matrix, Φ, is a diagonal matrix contained in the set of diagonal matrices that has all possible combinations and permutations of +1 and -1 on the diagonal. These matrices represent the possible directions of variation (positive or negative) of each of the real uncertainties. Use of the upper bound for real parameter variations yields not only the minimum size of Δ that can destabilize the system, but also the "worst case" direction for each individual variation. However, the structured singular value for real parameter variations is even with respect to Φ (i.e., $\mu_r(\Phi) = \mu_r(-\Phi)$).

Therefore, the "worst case" direction is subject to interpretation with respect to a scalar multiplier of ± 1.

The structured singular value analysis method can also be used to study the effect of isolated, single-valued nonlinear elements on system stability. If a sector can be drawn around the graph of a nonlinear element, then the structured singular value can be used to determine if the sector-bounded nonlinearity can destabilize the closed-loop system. References [37] and [38] describe analysis of nonlinear saturation using structured singular value analysis and sector-bounding methods, respectively.

Whether the matrix Δ represents linear or sector-bounded nonlinear elements, the structured singular value analysis gives only the minimum size of Δ that can destabilize the closed-loop system. Although some frequency information is obtained (since μ_r is a function of frequency), the method does not reveal the character of the instability that may result if the bound on Δ is exceeded. For example, it is not known whether the resulting divergence is purely exponential or oscillatory.

3.5.2 Numerical Algorithms

MATLAB™ contains two routines (in the Robust Control Systems toolbox) to calculate the upper bound on the structured singular value (*ssvbode* and *perron*). Both of these algorithms compute the structured singular value bound of Equation (3-9) which considers complex uncertainties. These algorithms are based on the work of Safonov [39] and can yield overly conservative estimates for systems with only real parameter variations.

For the immediate purpose of analyzing pilot/aircraft systems, only real uncertainties have been considered. Therefore, an algorithm based on that outlined by Reference [35] has been written to calculate the bound of Equation (3-10). The algorithm outline is given in Figure 3-5.

The maximum (real) structured singular value over all frequencies will be denoted μ_r and will be used to define the maximum allowable variation while guaranteed stability is

Algorithm to Compute Upper Bound on the
Structured Singular Value for Real Parameter Variations

1. Define frequency range of interest, $\omega_i \leq \omega \leq \omega_f$.

2. Set up 2^q x q matrix (Φ_T) whose rows account for the possible combinations and permutations of +1 and -1 (q = number of uncertainties).

3. At each ω,

   a) Calculate the transfer function matrix at $s = j\omega$, i.e. $M(j\omega)$.
   b) Use Osborne's technique to find D.
   c) For each row , k , in Φ_T ,
      1) Calculate diagonal Φ matrix as
         Φ = diag[k^{th} row of Φ_T].
      2) Find $\sigma_{max}[(DM(j\omega)D^{-1}\Phi + (DM(j\omega)D^{-1}\Phi)^T)/2]$.
         Store result as SV(k).
   d) Find the maximum value in SV(k) calculated above.
      This represents $\mu_r(M,\omega)$ at this frequency.

4. Plot the $\log(\mu_r(M,\omega))$ versus $\log(\omega)$.

Figure 3-5. Algorithm for Structured Singular Value Computation.

maintained. Assuming a diagonal uncertainty matrix (Δ=diag[$\delta_1,\delta_2,...,\delta_q$]), the closed-loop system will remain stable as long as the magnitude of each individual uncertainty is less than $1/\mu_r$ (i.e., $|\delta_i| < 1/\mu_r$).

3.5.3 Verification

To ensure that the stability robustness algorithms work correctly, an analysis of two configurations of the HAVE PIO database [13] was conducted. The flight test database given in Reference [13] provides experimental data which can be used to evaluate (longitudinal) PIO prediction methods. The experiments were conducted using the USAF/Calspan variable stability NT-33 aircraft. The 18 aircraft/flight control system configurations were evaluated in landing approach tasks. The four baseline configurations (H2-1, H3-1, H4-1, H5-1) were chosen to have different short period dynamics that all met MIL-F-8785C Level 1 boundaries for Category C landing approach. The phugoid

and lateral/directional characteristics, which all met Level 1 requirements, were held constant. PIO ratings, Cooper-Harper pilot ratings, and pilot comments were obtained.

For the current purpose, Configurations H2-1 and H2-5 were modified to include a first order actuator as shown in Figure 3-6. Table 3-1 gives the vehicle and pilot model parameters used in the analysis. The pilot model parameters were chosen using rules from the Neal-Smith criteria [2].

The two dynamic effects of interest are a simultaneous change in pilot gain and control surface actuator rate limiting. The rate limit is modeled by a saturation element in the actuator model and is represented by an equivalent, but variable, gain. A representation of the SIMULINK™ diagram used to define M(s) is shown in Figure 3-7. The first variation represents a percentage change in the pilot gain while the second represents a percentage change in the unity gain (L = 1) model of the saturation element.

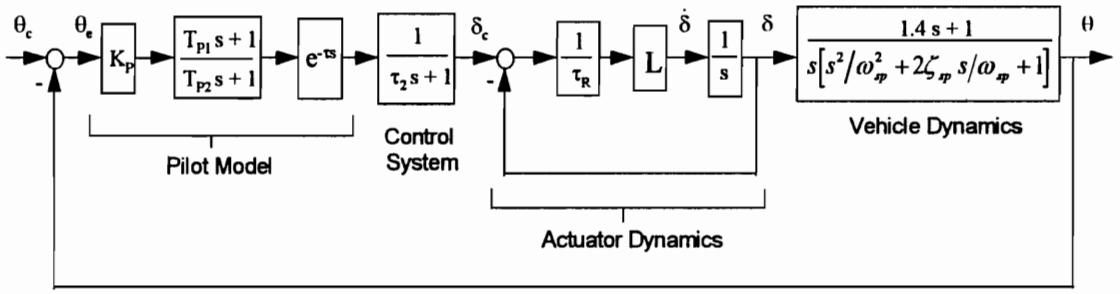

Figure 3-6. HAVE PIO Configuration Model Modified to Include Actuator Dynamics.

Table 3-1. Vehicle and Pilot Model Parameters for Modified HAVE PIO Configurations.

Configuration	ω_{sp} / ζ_{sp} (rad/s/-)	τ_2 (s)	τ_R (s)	L	K_P	T_{P1} (s)	T_{P2} (s)	τ (s)
H2-1	2.4 / 0.64	0	0.05	1.0	0.74	0.27	0	0.3
H2-5	2.4 / 0.64	1.0	0.05	1.0	0.52	2.37	0	0.3

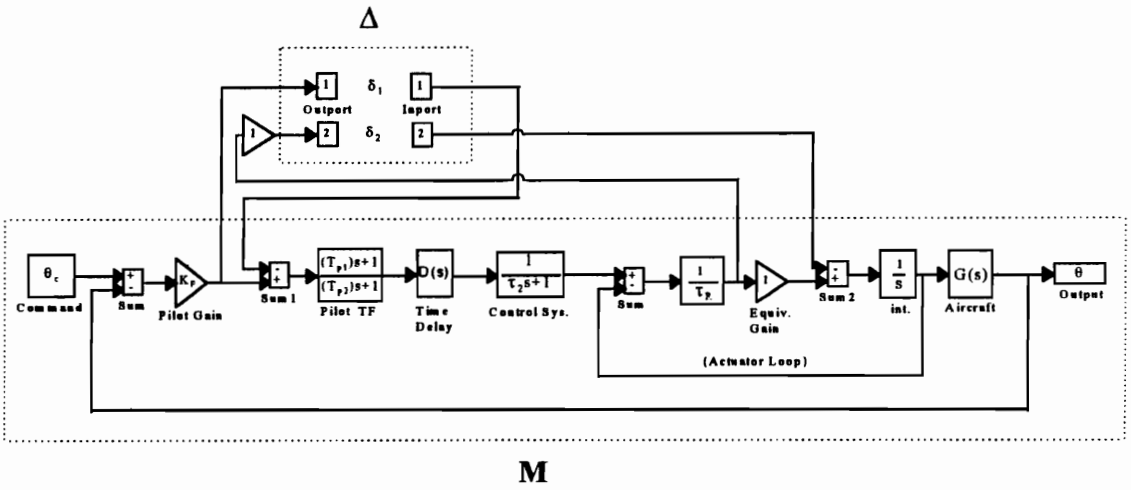

Figure 3-7. SIMULINK™ Diagram Used to Define M(s) for HAVE PIO Configurations.

Figure 3-8 shows the inverse real structured singular value calculation of Equation (3-10) for both configurations. The minimum of the inverse structured singular value plot reveals the largest bound on δ_1 and δ_2 (from Figure 3-7) before instability is possible. The minimum value is 0.56 for configuration H2-1 and 0.08 for configuration H2-5. The structured singular value calculation of Equation (3-10) also reveals the direction of the worst case variation. At the frequency where the minimum is found, the matrix Φ that maximized (3-10) is $\Phi = \text{diag}[-1, +1]$. As would be expected, the worst case variation in pilot gain is an increase of $(1+ \delta_1)$ and the worst case gain variation due to rate limiting is $(1- \delta_2)$. Due to symmetry, the same bounds are found with $\Phi = \text{diag}[+1, -1]$. This case is neglected because δ_2 is known to vary only between zero and +1.

The stability boundary calculated from the real structured singular value analysis of configurations H2-1 and H2-5 are shown in Figures 3-9 and 3-10 respectively. The shaded blocks represent values for pilot gain and equivalent gain due to rate limiting for which the structured singular value analysis guarantees stability. A direct calculation of the system poles yields the stability boundaries shown by the solid curves. The dashed lines represent the nominal value of the pilot gain in each case. The nominal value for the

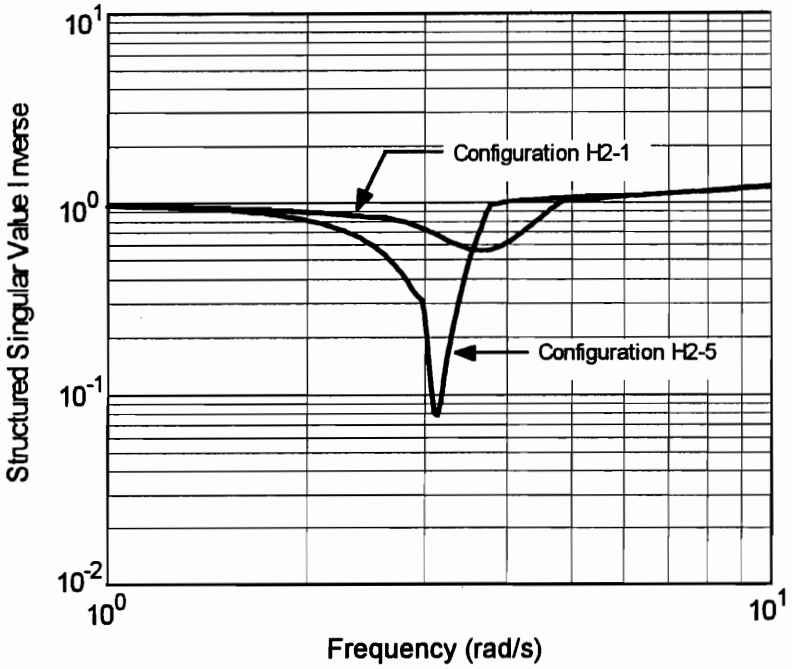

Figure 3-8. Inverse Structured Singular Value of M(s).

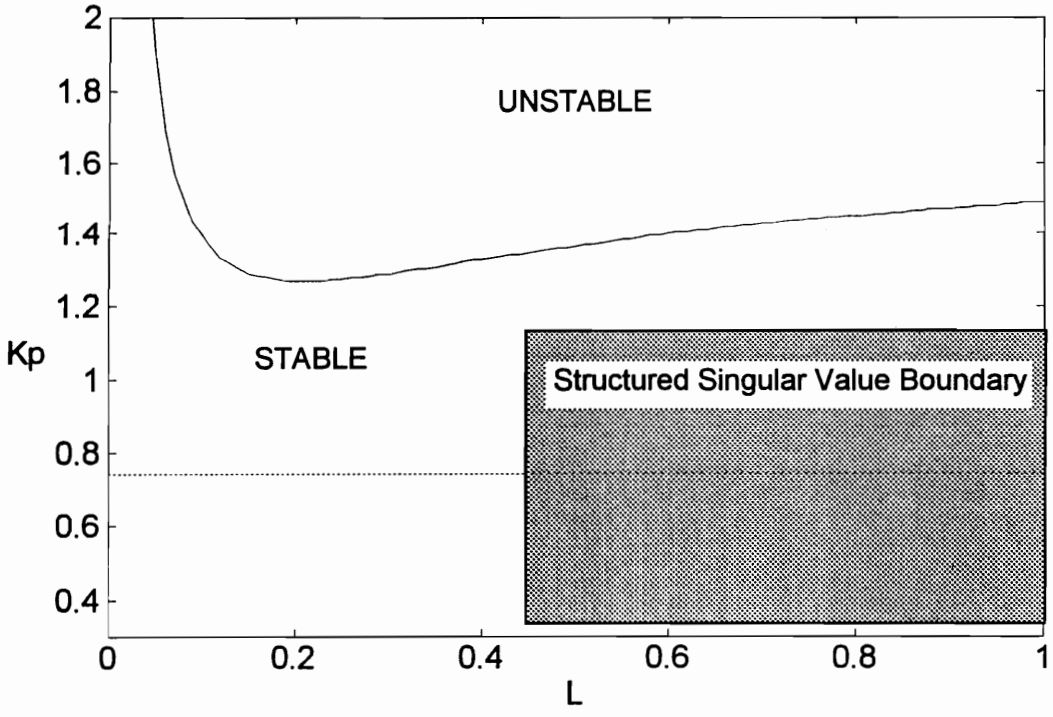

Figure 3-9. Stability Boundary For Configuration H2-1.

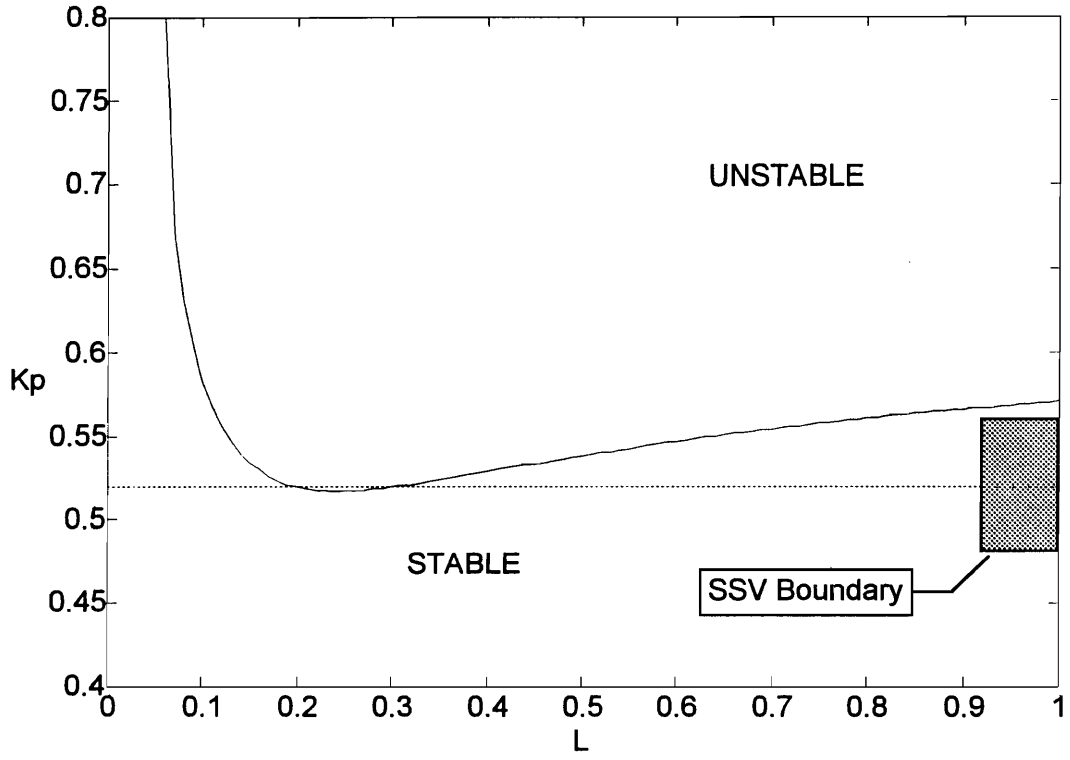

Figure 3-10. Stability Boundary for Configuration H2-5.

equivalent gain due to rate limiting is L = 1. Figures 3-9 and 3-10 illustrate how well the structured singular value approximation fills the stable region in the parameter space. The corners of the structured singular value boundaries closely approach the curves separating the stable and unstable regions in the parameter space indicating the structured singular value is a good approximation to the actual stability boundary.

Recall, Configuration H2-1 was rated PIO resistant while Configuration H2-5 was rated PIO prone. Application of the Smith-Geddes and Mitchell-Hoh criteria in Chapter 2 correctly predicted the susceptibility of these configurations. The results of the stability robustness analysis are consistent with the previous results. Since Configuration H2-1 can tolerate greater parameter variations while maintaining closed-loop system stability, it is expected to be more PIO resistant than Configuration H2-5.

3.5.4 Summary

When $\Delta=0$, the transfer function matrix, M(s), represents the nominal system dynamics. When the uncertain parameters are known to vary over a given range, they are usually scaled such that $-1 \leq \delta \leq 1$ encompasses the given variation. With a scaled system and $1/\mu_r \geq 1$, the closed-loop system can handle the given variation and remain stable. If $1/\mu_r \leq 1$, then the system can tolerate variations up to at least $\delta = 1/\mu_r$ while maintaining system stability. For the case of a variation in an equivalent gain representing a saturation element, the value of $1/\mu_r$ represents the percent saturation of the element. That is, the system can tolerate an input to a nonlinear element up to $100*\delta/(1-\delta)$ percent greater than the saturation limit while guaranteed stability is maintained.

3.6 Multivariable Describing Function Analysis

Some researchers have noted that PIOs are analogous to limit cycles [28 and 29]. A limit cycle is an unforced, self-sustained oscillation of a nonlinear system. The dynamics associated with the pilot/aircraft interaction are fundamentally nonlinear. In fact, both the pilot and aircraft are very complicated nonlinear systems. Graham and McRuer also note that nonlinear friction and hysteresis characteristics of early jet fighter flight control systems led to serious PIOs [28]. Thus, methods for predicting limit cycles for nonlinear systems are included in the unified PIO analysis method defined herein.

A useful class of nonlinear systems includes those with nonlinearities isolated as separate entities while the remaining linear elements are represented in lumped-parameter form. For this particular class of systems, an analysis based upon quasi-linear harmonic approximations is readily completed. The quasi-linear approximations are usually known as describing functions [40 and 41]. For PIO analysis, a describing function approach is particularly attractive as it has close ties with linear frequency-domain stability analysis. In addition, most of the existing PIO analysis methods discussed previously are also based on control-theoretic, frequency-domain methods.

3.6.1 Basic Theory

Assume the input to a single-input, single-output nonlinear element is sinusoidal with a given amplitude and frequency. The output of the nonlinear element will generally not be sinusoidal, but will be periodic with the same period as the input sinusoid. If the output wave is analyzed in terms of its Fourier components, the fundamental component can be related to the input in familiar terms of an amplitude ratio and a phase angle. The complex ratio of the fundamental component of the output to the input is defined as the sinusoidal input describing function (SIDF) [41].

For a sinusoidal input to the nonlinear element, $x(t) = \alpha \sin(\omega t)$, the output $y(t)$ is expressed in terms of its Fourier series. Namely,

$$y(t) = a_0 + \sum_{n=1}^{\infty} (a_n \cos n\omega t + b_n \sin n\omega t) \tag{3-11}$$

where,

$$a_n = \frac{1}{\pi} \int_0^{2\pi} y(t) \cos n\omega t \, d(\omega t)$$

$$b_n = \frac{1}{\pi} \int_0^{2\pi} y(t) \sin n\omega t \, d(\omega t)$$

For a skew symmetric nonlinearity, $a_0 = 0$ and the fundamental component of the output becomes,

$$y_1(t) = a_1 \cos \omega t + b_1 \sin \omega t \tag{3-12}$$

The describing function is then given by,

$$N(\alpha, \omega) = \frac{\sqrt{a_1 + b_1}}{\alpha} \angle \phi_1 \quad , \phi_1 = \tan^{-1}\left(\frac{a_1}{b_1}\right) \tag{3-13}$$

where a_1 and b_1 are obtained using the integral expressions in (3-11). In general, the describing function can depend on both the amplitude and frequency of the input signal. However, when the nonlinearity contains no energy storage element, N is a function of amplitude only [42]. All simple (single valued) nonlinearities and many complex nonlinearities have describing functions which are frequency invariant. Table 3-2 lists four useful nonlinearities and their frequency invariant describing functions.

Table 3-2. Four Nonlinearities and the Corresponding Sinusoidal Input Describing Functions.

Nonlinear Element	Sinusoidal Input Describing Function
Saturation 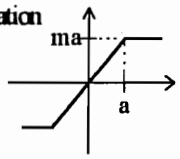	m (for $\alpha/a \le 1$) $\frac{2m}{\pi}\left[\sin^{-1}(a/\alpha)+(a/\alpha)\sqrt{1-(a/\alpha)^2}\right]$ (for $\alpha/a \ge 1$)
Dead-zone 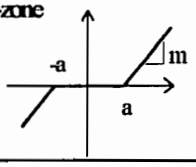	0 (for $\alpha/a \le 1$) $m-\frac{2m}{\pi}\left[\sin^{-1}(a/\alpha)+(a/\alpha)\sqrt{1-(a/\alpha)^2}\right]$ (for $\alpha/a \ge 1$)
Contactor 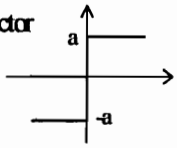	$\frac{4a}{\pi\alpha}$
Preload 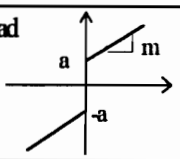	$m+\frac{4a}{\pi\alpha}$

Figure 3-11 shows an example of replacing a nonlinear element by its SIDF resulting in a quasi-linear feedback system. The remnant consists of the higher harmonics of the Fourier series of the output (terms with $n > 1$ in Equation (3-11)). The output of the actual nonlinearity is equal to the SIDF, multiplied by the input, plus the remnant. In considering only the fundamental harmonic when developing the describing function, it is automatically assumed that the remnant has little affect on the system output. This assumption holds if the linear part of the system is sufficiently low-pass to attenuate the higher harmonics introduced by the remnant. Also, the maximum amplitude present in the remnant is normally much less than the magnitude of the fundamental harmonic. For the case of a saturation nonlinearity and a K/s type plant, Reference [41] states the largest term in the remnant (which is the third harmonic) is never more than 28% of the amplitude of the fundamental component of the output of the nonlinearity. When attenuated by the

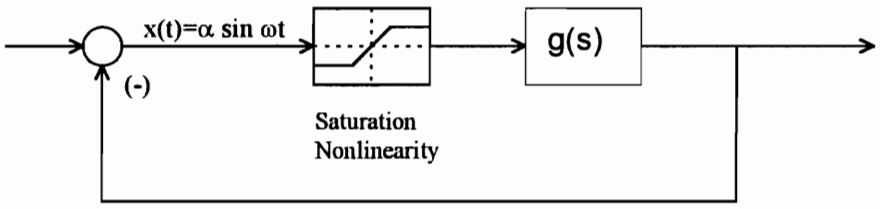

a) Nonlinear System

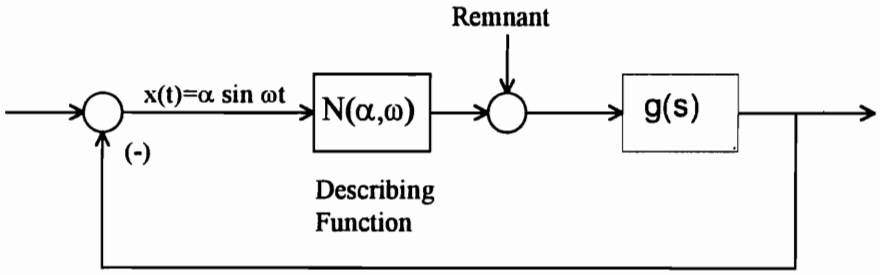

b) Quasi-Linear System

Figure 3-11. Replacement of a Nonlinear Element by a Sinusoidal Input Describing Function.

integrator, the amount of the third harmonic present in the error signal , x(t), as compared to the fundamental is not more than 9%. This value is an indication of the error introduced by ignoring the contribution of the remnant.

To remain consistent with the concept of a unified analysis diagram that was put forth in Section 3.3, the process depicted in Figure 3-11 must be modified. Note that if the describing function in Figure 3-11 were set equal to zero, the feedback loop would be broken and the nominal system would not be retained. Therefore, it is necessary to represent each given nonlinear element as a nominal linear element connected with a new "complementary" nonlinear element. For example, the saturation nonlinearity can be replaced by the combination of a linear gain and a dead-zone nonlinearity as depicted in Figure 3-12. The nominal linear system is now given by a gain that equals the slope of the linear portion of the saturation element. The "complementary" nonlinear portion is taken

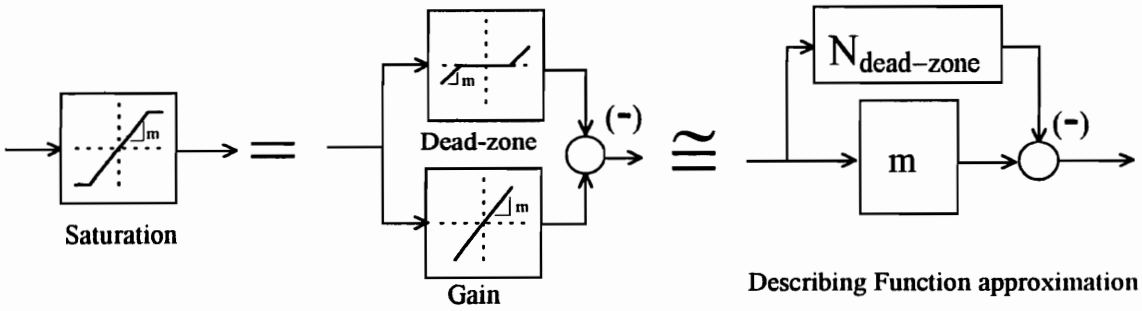

Figure 3-12. Representation of a Nonlinear Element by a Combination of Complementary Elements.

as a dead-zone. Note the input signal to the dead-zone nonlinear element is the same as the input signal to the original saturation element.

While it is possible to tabulate a set of complementary nonlinear elements, it is entirely unnecessary. From a strictly mathematical point-of-view, the describing function for a group of nonlinear elements connected in parallel is simply equal to the sum of the describing functions for the individual elements [40]. For the purposes of PIO analysis, the given nonlinear element will be replaced by a corresponding linear gain connected in parallel with a new complementary nonlinear element, as depicted in Figure 3-13. For this situation, the describing function for the complementary nonlinear element is given by,

$$N_{comp} = L - N_{given} \tag{3-14}$$

It is therefore a rather trivial matter to calculate the correct describing function for use in the unified analysis diagram. This replacement not only yields the nominal system when $N_{comp} = 0$, but it is also yields a representation of the same form as the equivalent gain representation used previously in stability robustness analysis (Figure 3-3). Also, the input to the "complementary" nonlinear element is the same as the input to the original nonlinear element so that the results of the describing function analysis are the same as before replacement.

Although the above discussion considers a single-loop system with a single nonlinearity, extension to a multi-loop multiple-nonlinearity system is straightforward. Let Δ from Figure 3-1 represent a diagonal matrix of nonlinear elements. In this case, M(s) represents

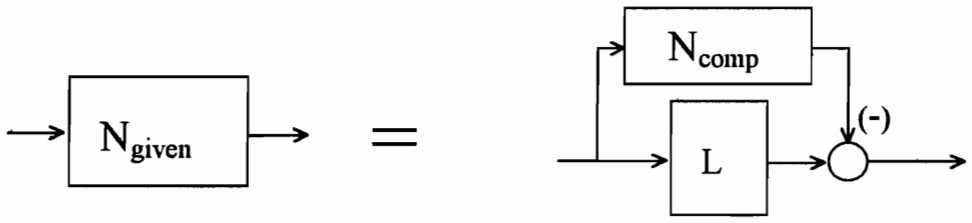

Figure 3-13. Replacement of a Given Nonlinear Element by a Combination of a Linear Gain and a Complementary Nonlinear Element.

the linear part of the system as seen by the nonlinear elements in Δ. Assume the input signal to each nonlinear element in Δ is sinusoidal and oscillating at the same frequency (ω). The input signals are given by,

$$x_i = \alpha_i \sin(\omega t + \theta_i) \tag{3-15}$$

To use describing function approximations, the linear part of the system, represented by M(s), is assumed to act like a low-pass filter so that superharmonic signal components can be neglected in the analysis. Under these assumptions, the nonlinear elements can be replaced by their sinusoidal-input describing functions (SIDF). Namely,

$$\Delta \rightarrow N(A,\omega) \tag{3-16}$$

where 'A' is a vector containing the amplitudes (α_i)of the sinusoids entering each nonlinear element and $N(A,\omega)$ is a diagonal matrix of describing functions made up of individual elements like those in Table 3-2, as modified by Equation (3-14).

In order to investigate the stability of the multivariable nonlinear feedback system, solutions of the system characteristic equation are considered. Since it is assumed that each feedback loop is oscillating at the same frequency, the Laplace operator in (3-7) can be replaced with $s=j\omega$. Equation (3-7) then becomes,

$$[I + M(j\omega)N(A,\omega)]\, x(j\omega) = 0 \tag{3-17}$$

Equation (3-17) represents the "harmonic-balance" equation for the system. Non-zero solutions to (3-17) predict the existence of limit cycles.

3.6.2 Numerical Algorithms

Since $x(j\omega) = 0$ represents a trivial solution to (3-17), many researchers have used the following determinant to predict limit cycles,

$$\det [I + M(j\omega)N(A,\omega)] = 0 \tag{3-18}$$

Alternatively, one could search for values of ω and A that yield one or more zero eigenvalues of $[I + M(j\omega)N(A,\omega)]$ or eigenvalues of $[M(j\omega)N(A,\omega)]$ equal to $-1+j0$ [43].

There are several computational methods available to aid in the search for limit cycle behavior. Besides searching (3-17) or (3-18) directly, Gray and Nakhla use Gershgorin bands as an eigenvalue check [44]. Gray and Taylor have developed a search method that considers each feedback loop in a sequential order, while systematically eliminating solution possibilities throughout the search [45]. Chang, et. al. have recently extended the sequential loop method of Gray and Taylor to include a homotopy algorithm with claims of global convergence [46]. At about the same time, Pillai and Nelson reported search method results based upon Newton-Raphson optimization methods [47].

The method of Chang, et. al. warrants further explanation as it is easily extended to the current M-Δ formulation. Also, the use of a linear homotopy to improve the convergence of the search algorithm is a desirable feature. When cast in the standard M-Δ form above, the set of nonlinear equations that Chang refers to as "auxiliary characteristic equations" reduce exactly to the harmonic-balance equations in (3-17). These equations can be rewritten as a set of n complex nonlinear equations (one for each nonlinear element) of the form,

$$f_i = x_i(j\omega) + \sum_{k=1}^{n} M_{ik}(j\omega)\, N_k(A_k,\omega)\, x_k(j\omega) = 0 \tag{3-19}$$

where $x_i(j\omega)$ is the result of replacing $s=j\omega$ in the Laplace transform of $x_i(t)$ of Equation (3-15). With some straightforward substitutions and cancellations, it can be shown that for numerical solution, $x_i(j\omega)$ in the above equation can be replaced by,

$$x_i(j\omega) \rightarrow x(A_i,\theta_i) = A_i e^{j\theta_i} \tag{3-20}$$

The existence of a limit cycle is then found by solving the system of n complex equations given in (3-19), with the substitution of (3-20), for the 2n unknowns $(A_1,\omega,A_2,\theta_2,\ldots,A_n,\theta_n)$. The phase angle of the sinusoid entering the first nonlinear element is taken to be zero $(\theta_1=0)$ without loss of generality.

When a good initial guess of the solution is available, the system of nonlinear equations can likely be solved by any method normally used for nonlinear systems (e.g., Newton-Raphson). However, since a sufficiently good guess is not always available, a homotopy method of solution is recommended. Define the homotopy H as,

$$\vec{H}(\vec{z},t) = (1-t)(\vec{z}-\vec{z}_0) + t\vec{f}(\vec{z}) \tag{3-21}$$

where $\vec{z}=(A_1,\omega,A_2,\theta_2,\ldots,A_n,\theta_n)$, t is an independent, real, scalar homotopy parameter, $\vec{z}_0$ represents the initial guess for $\vec{z}$ at t=0, and $\vec{f}$ is defined by (3-19). The solution of $\vec{H}=\vec{0}$ for all $t\in[0,1]$ forms a space trajectory. For t = 0, the solution is simply $\vec{z}=\vec{z}_0$. At t = 1, the solution is that desired $\vec{H}=\vec{f}=\vec{0}$. Therefore, if one can trace the solution $\vec{H}=\vec{0}$ from t = 0 to t =1, a desired solution will have been reached. Multiple solutions may exist when $\vec{f}$ is nonlinear. One way to trace a solution is to integrate the differential equation obtained by taking the total derivative of $\vec{H}$ with respect to t. Namely,

$$\frac{d\vec{H}(\vec{z},t)}{dt} = \frac{\partial\vec{H}(\vec{z},t)}{\partial t} + \frac{\partial\vec{H}(\vec{z},t)}{\partial\vec{z}}\frac{d\vec{z}}{dt} = 0 \tag{3-22}$$

or,

$$\frac{d\vec{z}}{dt} = -\left[\frac{\partial\vec{H}(\vec{z},t)}{\partial\vec{z}}\right]^{-1}\frac{\partial\vec{H}(\vec{z},t)}{\partial t} \tag{3-23}$$

where,

$$\frac{\partial\vec{H}(\vec{z},t)}{\partial\vec{z}} = (1-t)I + t\frac{\partial\vec{f}(\vec{z})}{\partial\vec{z}} \qquad \frac{\partial\vec{f}(\vec{z})}{\partial\vec{z}} = \begin{bmatrix} \frac{\partial f_1}{\partial z_1} & \cdots & \frac{\partial f_1}{\partial z_n} \\ \vdots & \ddots & \vdots \\ \frac{\partial f_n}{\partial z_1} & \cdots & \frac{\partial f_n}{\partial z_n} \end{bmatrix}$$

$$\frac{\partial\vec{H}(\vec{z},t)}{\partial t} = -(\vec{z}-\vec{z}_0) + \vec{f}(\vec{z})$$

The necessary partial derivatives can be computed numerically if desired. When a solution for $\vec{z}$ is obtained, it indicates the frequency of the resulting oscillation along with the input amplitudes and phase angles into each isolated nonlinear element.

Since the solution of a limit cycle governs the behavior of a dynamic system, it is reasonable to speak of the stability of the limit cycle. When a system that has fallen into a stable limit cycle is perturbed slightly from the limit cycle condition, the system will return to the limit cycle. If a system were able to operate at an unstable limit cycle condition and was perturbed slightly from that condition, it would not return. The resulting behavior could be divergent, asymptotically stable, or could converge to a different (stable) limit cycle. For this reason, an unstable limit cycle cannot be observed experimentally. According to Chang [46], the stability of the limit cycle is determined by considering a real perturbation in the limit cycle frequency, $s = \sigma + j\omega$. The limit cycle will be stable as long as,

$$d\sigma/dA_1 < 0 \tag{3-24}$$

Graham [41] further distinguishes between soft and hard self-excitation of a stable limit cycle. Soft self-excitation exists when any nonzero initial condition will result in the sustained oscillation of the stable limit cycle. Soft self-excitation is common in systems where the linear transfer function matrix describes an unstable system. On the other hand, hard self-excitation exists when the input and subsequent removal of a certain amplitude or waveform signal is required to excite the oscillation.

3.6.3 Verification

To ensure the multivariable describing function analysis methods work as desired, an analysis based on that of Reference [15] is given. Three alternative longitudinal and lateral/directional limited authority back-up control systems for the F-4C are considered. The research of Reference [15] was undertaken to develop analytical techniques for determining the minimum levels for the back-up control system parameters. A companion project utilized piloted, fixed-base simulation to empirically determine the minimum levels for the back-up control system parameters.

A PIO analysis is conducted in the reference by applying sinusoidal input describing function theory. Susceptibility to initiating an oscillation is investigated by assuming the pilot controls the airplane in a normal way except that the amount of lead equalization generated by the pilot is reduced. The ability to sustain the oscillation is investigated by assuming the pilot behaves in a synchronous manner. The dynamic model contains two types of nonlinear elements: 1) actuator rate and displacement limits for a fully powered manual control system and 2) direct manual control authority limits determined by pilot strength or by control surface travel stops.

Figure 3-14 shows the block diagram for the longitudinal back-up control system A. The shorthand notation used in Figure 3-14 is $(\omega) = (s+\omega)$. The parameters for the pilot loop closures for the configuration in Figure 3-14 are given in Table 3-3. The pilot model is used as given in Reference [15] and was originally developed by the authors using techniques based on the crossover pilot model.

Figure 3-15 shows the deflection and rate limited actuator model used in the describing function analysis. Reference [15] develops a single SIDF for the combination of the two nonlinear elements represented in Figure 3-15 and uses graphical means to predict the existence of limit cycles. However, the methods introduced in this section can be employed to treat the two nonlinear elements as separate entities. The SIMULINK™ diagram needed to define M(s) is given in Figure 3-16. The first *inport/outport* pair corresponds to the actuator rate limit while the second *inport/outport* pair corresponds to the actuator deflection limit.

Table 3-3. Model Parameters for the F-4C.

K_u = 30.0 unit thrust/(ft/sec)	K_θ = -0.393	$K_{\dot{\theta}}$ = -0.244 sec
K_d = -0.03 deg/ft	$K_{\dot{d}}$ = -0.0015 deg/(ft/sec)	τ_T = 0.33 sec
τ_s = 0.2 sec	ω_n = 10 rad/sec	ω_2 = 0.5 rad/sec
ω_3 = 10 rad/sec	ω_4 = 2.25 rad/sec	

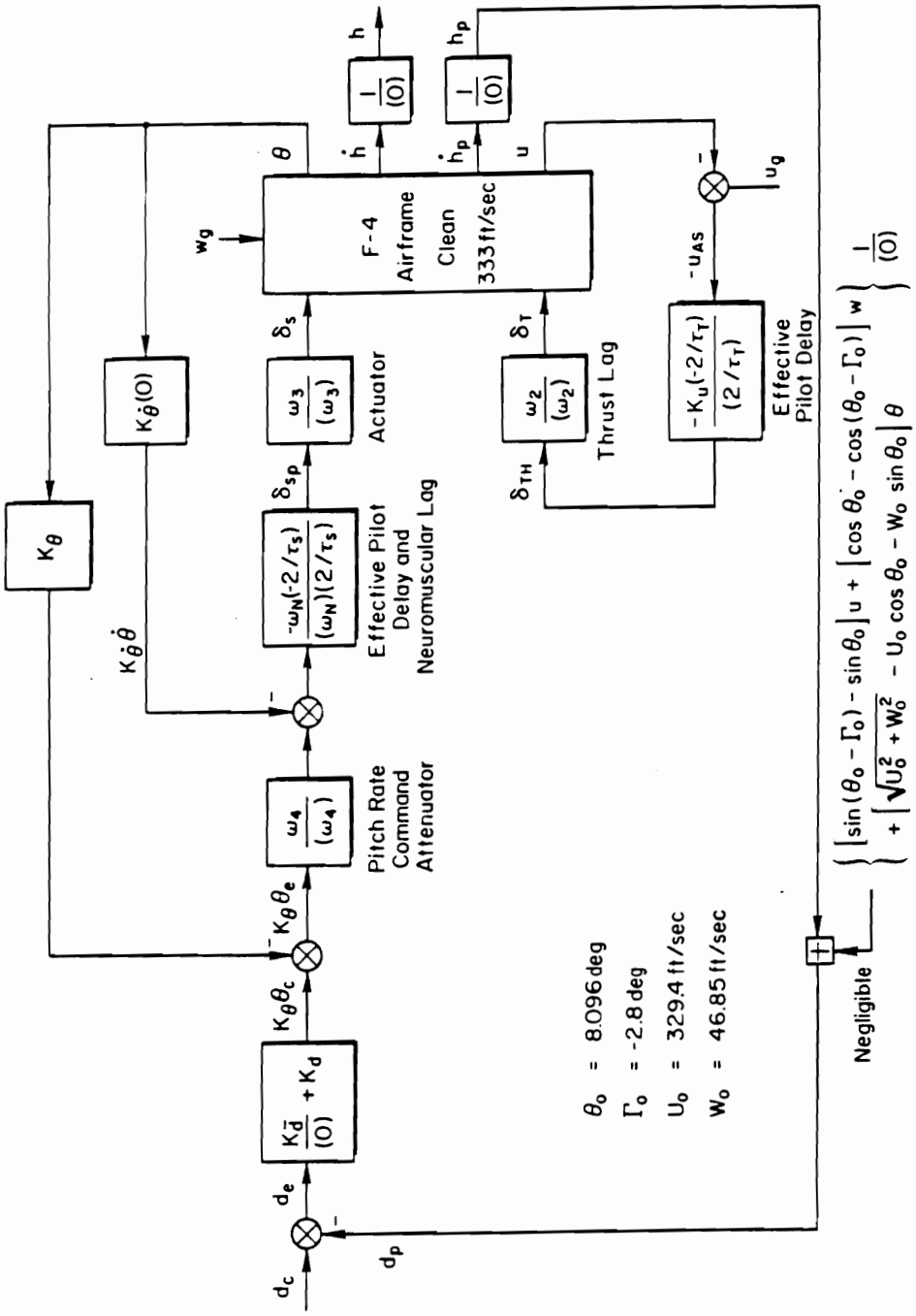

Figure 3-14. Longitudinal Block Diagram for F-4C Back-up Control System A [15].

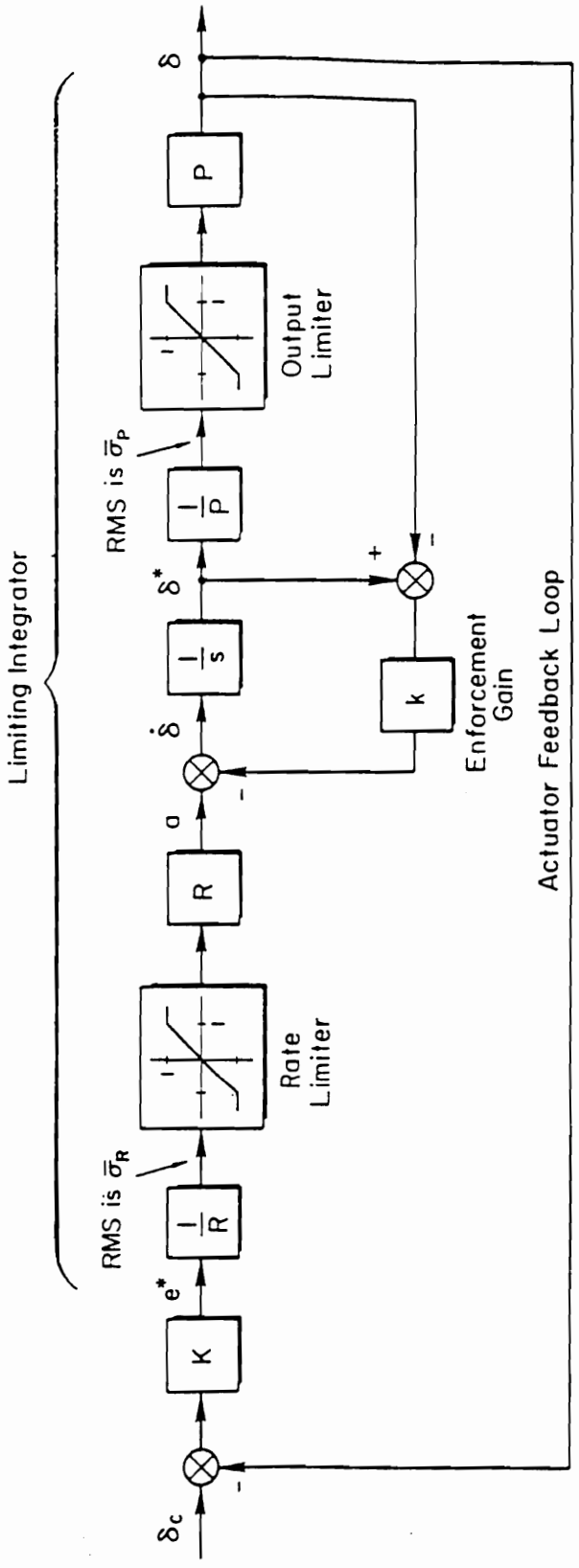

Figure 3-15. Rate and Position Limited Actuator [15].

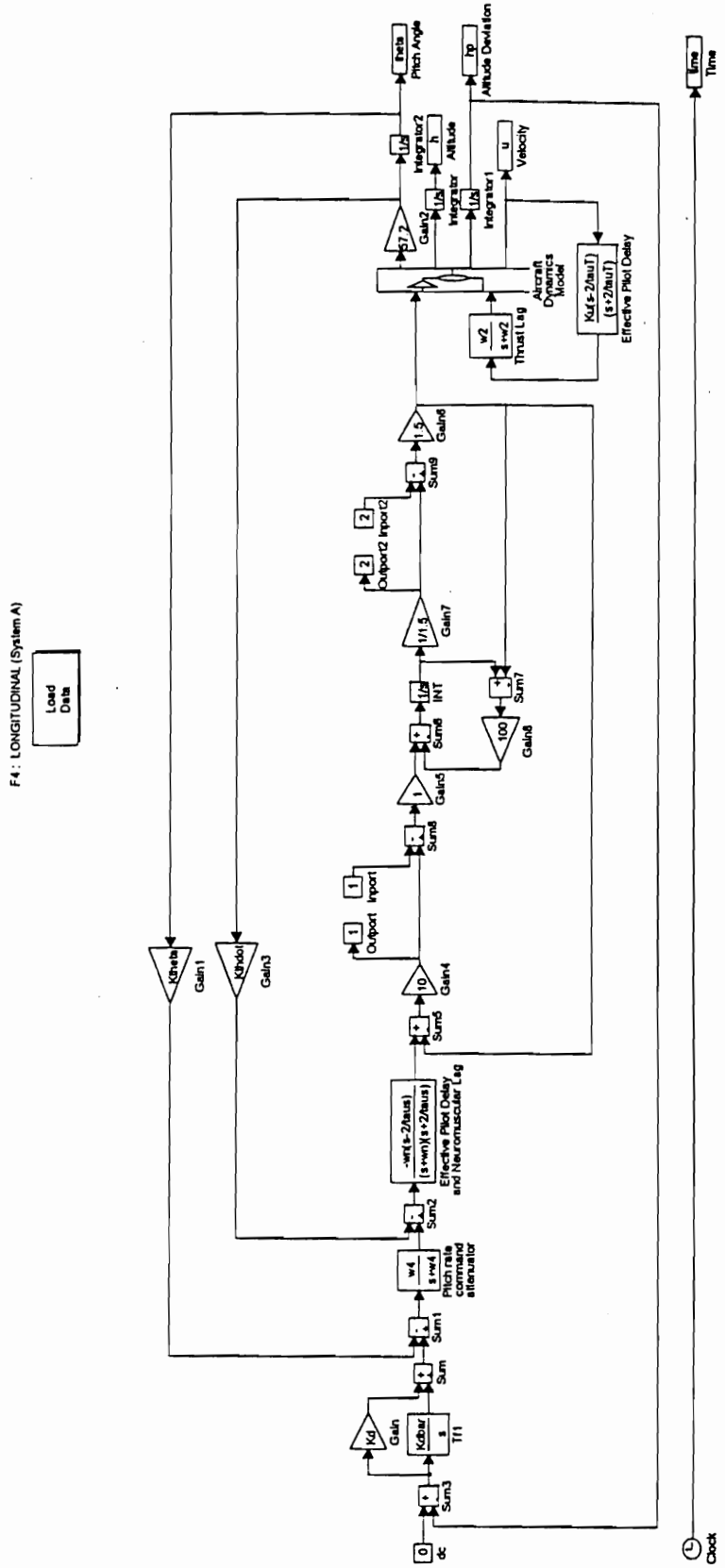

Figure 3-16. SIMULINK™ Diagram to Define M(s) for the F-4C.

The results of applying the limit cycle search algorithms given in Section 3.6.2 are presented in Tables 3-4 and 3-5. Also shown in the tables are the results from the given reference. A dash in a column indicates that no limit cycle is predicted for the corresponding configuration. The tables show results for all configurations studied in Reference [15] though only longitudinal back-up control system A has been presented in any detail here. The results found with the current method agree extremely well with those given in the reference. The newly calculated amplitudes vary by less than 5% from those given except for lateral/direction system C which varied by 10%. The predicted frequencies vary by less than 3% from those given in the reference. Since the amplitudes have been scaled such that values greater than unity indicate limiting of the saturation elements, it is seen that only lateral/directional system A is simultaneously rate and position limited.

Table 3-4. Comparison of Limit Cycle Results for the Longitudinal Systems.

			Reference [15]			Multivariable Analysis			
Back-up System	τ_s (sec)	$K_{\dot{\theta}}$ (sec)	Rate Amp.	Deflection Amp.	ω (rad/s)	Rate Amp.	Deflection Amp.	ω (rad/s)	Phase Difference (deg)
A	0.2	0	12.3	-	1.1	12.2	0.79	1.07	-90
A	0	0	10.0	-	1.2	10.4	0.71	1.19	-90
B	0.2	0	-	1.3	1.4	-	1.30	1.43	-
B	0	0	-	-	-	-	-	-	-

Table 3-5. Comparison of Limit Cycle Results for the Lateral/Directional Systems.

			Reference [15]			Multivariable Analysis			
Back-up System	τ_a (sec)	$K_{\dot{\phi}}$ (sec)	Rate Amp.	Deflection Amp.	ω (rad/s)	Rate Amp.	Deflection Amp.	ω (rad/s)	Phase Difference (deg)
A	0.2	0	15.0	1.0	0.14	14.3	1.01	0.14	-4
B	0.2	0	-	4.3	0.13	-	4.4	0.13	-
C	0.2	0	-	5.0	0.23	-	4.5	0.23	-

Figure 3-17 shows time response simulation results for longitudinal control system A, with the effective pilot delay $\tau_s = 0.2$. The resulting amplitudes, frequency, and phase agree with those predicted by the multivariable analysis. Figures 3-18 and 3-19 show the altitude-altitude rate phase plane for the same configuration as Figure 3-17 for small and large initial conditions respectively. The resulting closed curves on the phase plane are characteristic of stable limit cycles and it is noted that the same closed curve is obtained for both initial conditions.

While Equation (3-19) can be searched directly using a nonlinear equation solver, often times a good initial guess is necessary to ensure convergence. For this reason, the homotopy method as described above is used as the first solution technique. Since the homotopy algorithm can be slow to converge when using numerical partial derivatives, and since nonlinear equation solvers can be quite rapid when in the neighborhood of a

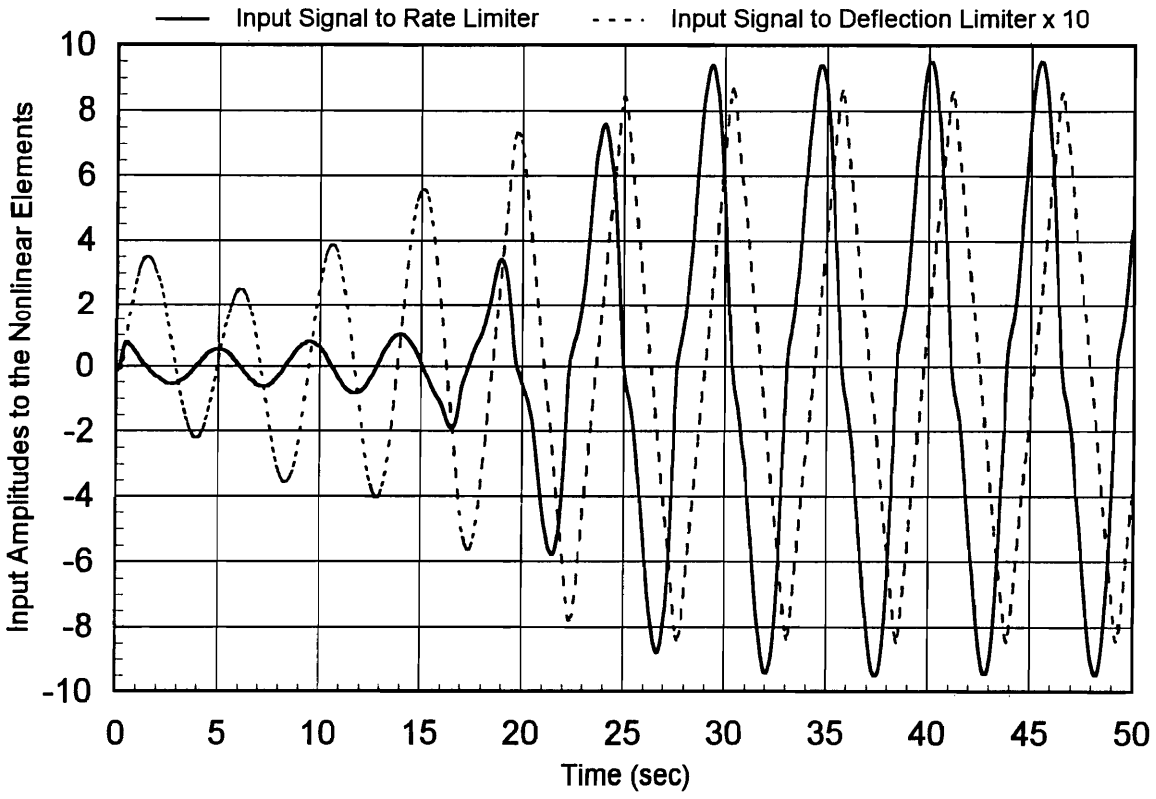

Figure 3-17. Simulation Results for F-4C.

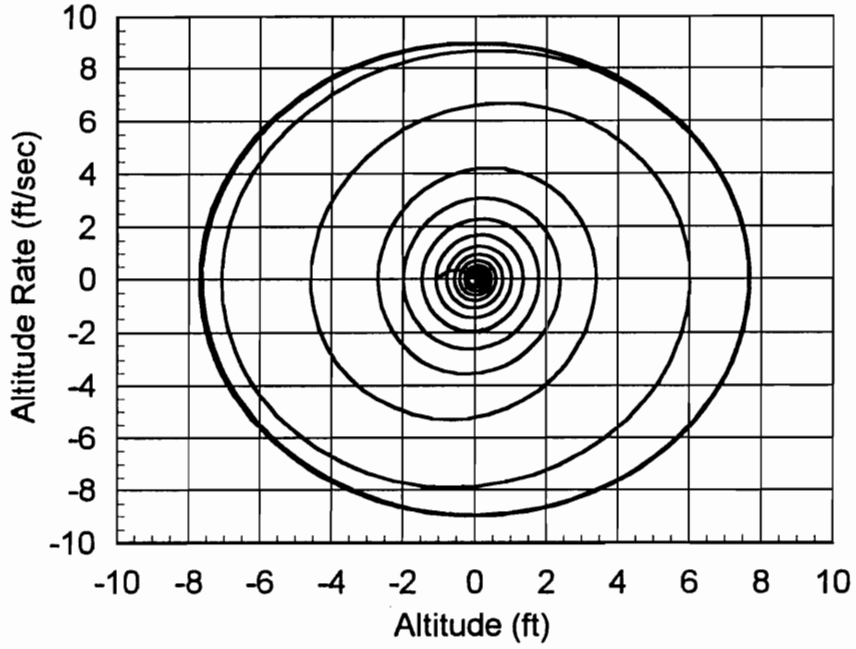

Figure 3-18. Altitude-Altitude Rate Phase Plane (Small Initial Condition).

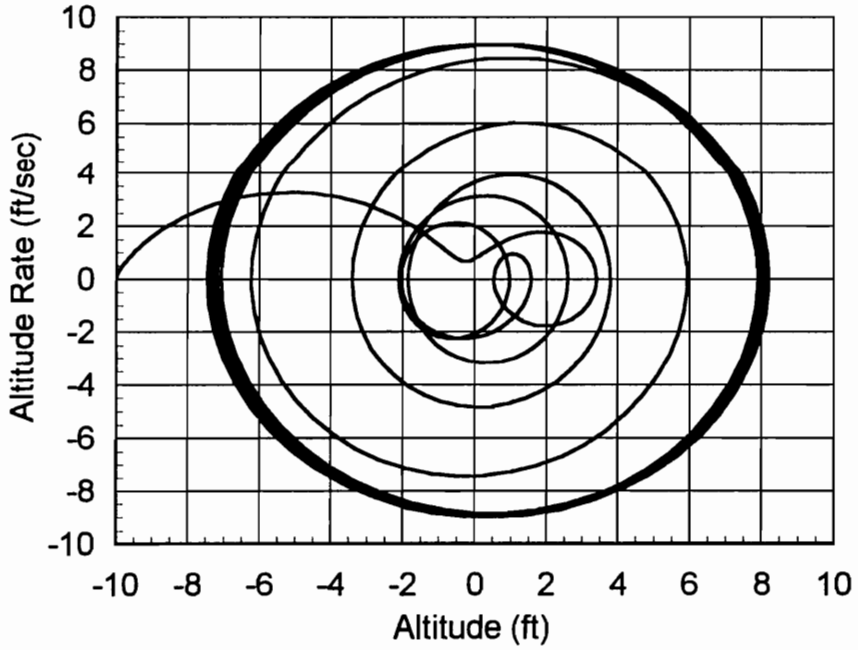

Figure 3-19. Altitude-Altitude Rate Phase Plane (Large Initial Condition).

solution, a combination of the two methods proved to be useful in obtaining the desired solution. A suitable initial guess is obtained from examining the stability robustness results. The homotopy equations are then integrated using a low tolerance to yield a new initial guess. Finally, the nonlinear equation solver is employed to yield a more accurate solution.

3.6.4 Summary

Describing function analysis provides more information about instability than structured singular value analysis because more information is known about how the model parameters vary. The structured singular value calculation yields a bound on the largest parameter variation or the largest sector bound of a nonlinearity. The describing function analysis, on the other hand, yields the magnitude and phase of resulting oscillations. However, the describing function analysis requires a fairly sophisticated search for solutions whereas computationally efficient approximations to the structured singular value are well-known. As a result, these two analysis methods are very complementary to the study of system stability (including pilot-induced oscillations).

Also, the existence of hard self-excitations may help explain why certain aircraft exhibit acceptable flying qualities for some pilots and yield severe PIOs for others. Recall, hard self excitation describes the condition where a certain amplitude or waveform of an input signal is necessary to excite the limit cycle. It is possible that the unlucky pilot just happened to input the necessary amplitude and waveform signal needed to excite the limit cycle behavior.

4 Unified PIO Analysis of the M2-F2

In order to fully exercise the unified PIO analysis method, it is desired to use the techniques to analyze an aircraft that has experienced in-flight PIOs. For the analysis to be meaningful, sufficient vehicle modeling data along with flight time histories of the oscillation events needs to be available. For these reasons, the M2-F2 lifting body vehicle is chosen as an example case study. All information for the M2-F2 is taken from Reference [6].

The M2-F2 is a half cone lifting body designed as part of the manned lifting body flight test program conducted in the 1960s. Basic research was being conducted at that time on manned reentry vehicles designed to maneuver and land unpowered at a specified location. The M2-F2 had a conventional fighter aircraft type cockpit with aerodynamic control being provided by upper elevon flaps, a lower flap, and twin rudders. A three view representation of the M2-F2 taken from Reference [6] is given in Figure 4-1. The upper elevon flaps provided coarse longitudinal trim and were deflected differentially (aileron deflection) to provide roll control. Because adverse yawing moment was produced by aileron deflection, a mechanical aileron-to-rudder interconnect was provided. The interconnect ratio was adjustable by the pilot. A stability augmentation system was used to improve damping in the pitch, roll, and yaw axes.

The M2-F2 was dropped from a B-52 at an altitude of 45,000 feet and a Mach number of about 0.6. Flight test maneuvers were performed during the unpowered descent to assess the handling characteristics of the vehicle. As a result of training on a six-degree-of-freedom fixed base simulator, the pilots were thoroughly familiar with the flight plan and predicted handling qualities of the research vehicle. The M2-F2 exhibited good handling qualities longitudinally, but the lateral/directional characteristics were consistently rated much lower; due largely to the appearance of a coupled roll spiral mode at low angles of attack.

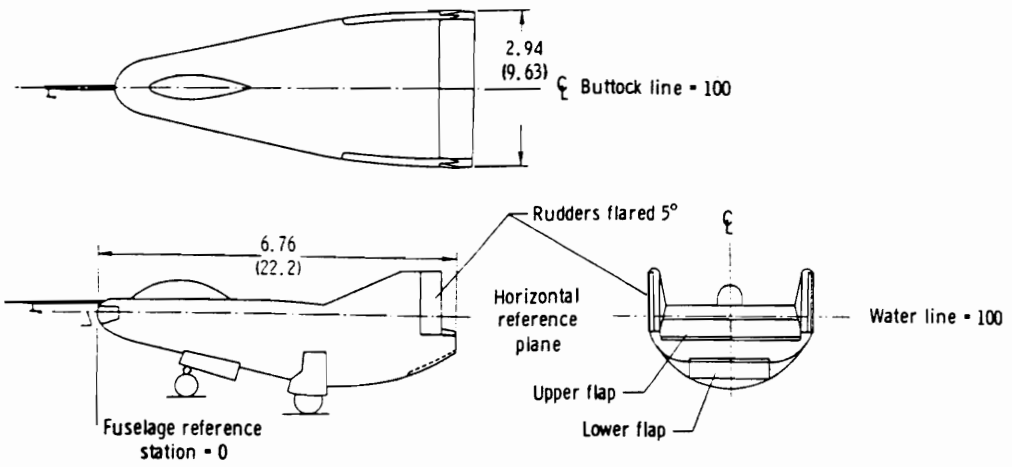

Figure 4-1. Three-View Drawing of the M2-F2. Dimensions in meters (feet) [6].

The vehicle experienced severe lateral/directional oscillations during three of its sixteen flights. Each of the oscillations occurred when the pilot was attempting to closely control the bank angle at slightly negative angles of attack. The PIO incident during the final flight contributed to a gear-up landing in which the vehicle was extensively damaged [6]. As the result of the accident, a center fin was added to the vehicle to improve the lateral/directional dynamics. The slightly redesigned vehicle was designated the M2-F3.

4.1 Develop Pilot Model

The task under consideration is the tight control of the bank angle and will be modeled as a compensatory tracking task. A Modified Optimal Control Model (MOCM) of the human pilot will be considered for this example. The pilot model is designed based on the linear transfer function of the controlled system. For simplification, and comparison to Reference [6], only the pilots aileron input is considered. This restriction should not pose a problem since piloted simulation analysis in Reference [6] indicated PIO for the situation of aileron only input as well as for coordinated aileron/rudder input during turn to final approach. A simplified block diagram of the situation under consideration is given in Figure 4-2. The MOCM code of Reference [12] was used to compute the pilot model. The parameters used in the MOCM model are shown in Table 4-1. The values are based on those given in Reference [48] for the roll axis.

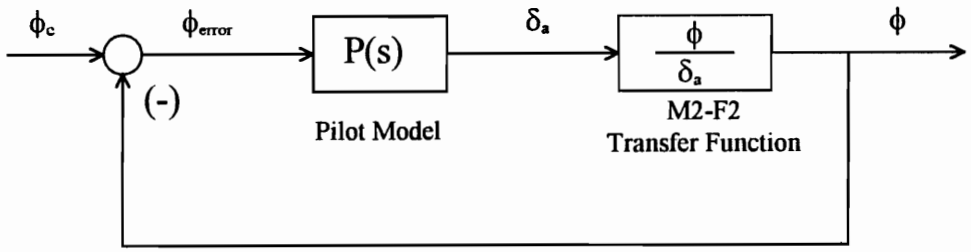

Figure 4-2. Block Diagram for Single Axis Tracking Task.

Table 4-1. MOCM Pilot Model Parameters.

Parameter	Value
time delay	0.2 sec
neuromuscular time constant	0.1 sec
observation noise-to-signal ratio	0.01
neuromotor noise-to-signal ratio	0.003
command disturbance filter	$13.31/(s^2+2(0.7)(0.5)s+(0.5^2))$

The optimal MOCM cost function is assumed to be given by,

$$J = \int_0^\infty \left[\phi_{error}^2 + \rho\dot{\delta}_a^2\right]dt \tag{4-1}$$

where ϕ_{error} is the bank angle error signal and δ_a is the pilot aileron command input. The control rate weighting, ρ, is chosen to achieve the desired neuromuscular time constant as described in Reference [23]. Note that the error rate is retained in the observation vector but is not weighted in the cost function (4-1).

4.2 Identify Dynamic Elements Suspected of Contributing to PIO

The next step in the closed-loop analysis is to identify those elements of the aircraft and stability augmentation system that are suspected of contributing to the potential for PIO. A block diagram of the M2-F2 lateral/directional flight control system is given in Figure 4-3. Since actuator rate limiting has been identified as a contributing factor in many previous PIO events, the rate limits of both the aileron and rudder actuators are considered in the analysis. Command authority limits were placed on the pilot input as well as both the roll and yaw SAS commands. These command limits, together with the actuator rate limits, comprise a total of five nonlinear elements that are considered possible contributors to PIO. The rate and command limits are given in Table 4-2.

Furthermore, since a mechanical aileron-to-rudder interconnect is needed to provide acceptable lateral/directional characteristics, it also poses a potential problem in terms of oscillation tendencies. This threat was recognized during the NASA fixed base simulations as depicted in Figure 4-4. Along with the aileron-to-rudder interconnect ratio, variations in the roll and yaw SAS gains are considered as linear elements of the vehicle suspected of contributing to undesirable oscillations.

In addition to elements of the aircraft and SAS, variations in the pilot model parameters are also considered. The underlying concept of the closed-loop analysis is that a PIO resistant aircraft will remain stable in the face of variations in the pilot model. Since increased pilot gain is often associated with the occurrence of PIO, variations in the pilot gain are considered in the analysis. While variations in other pilot model parameters (such as pilot time delay) could be examined, only a variation in pilot gain is included in the analysis of the M2-F2.

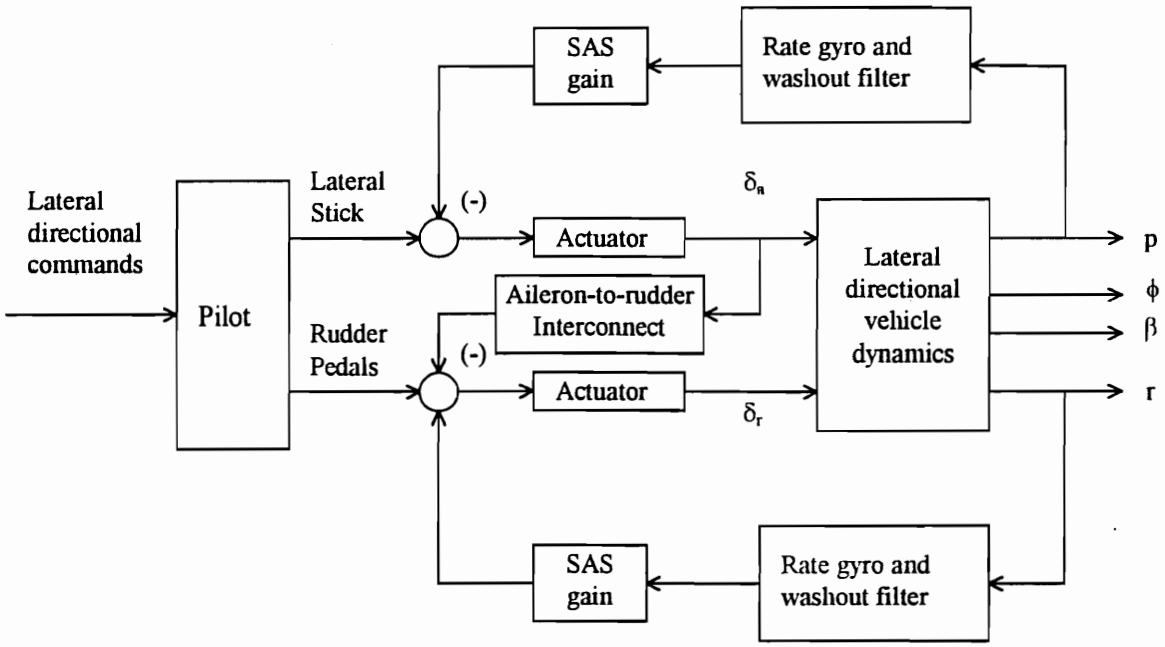

Figure 4-3. Block Diagram of M2-F2 Lateral/Directional Control System.

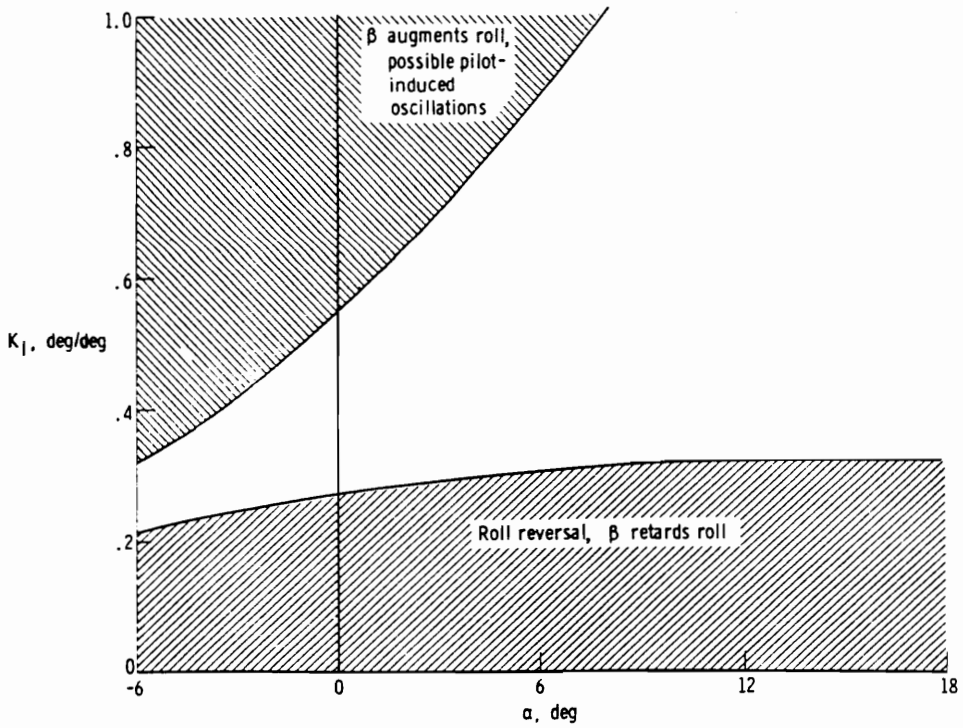

Figure 4-4. Simulator Predicted Regions of Lateral Control Problems as a Function of Angle of Attack and Aileron-to-Rudder Interconnect Ratio [6].

Table 4-2. M2-F2 Actuator Rate and Command Authority Limits.

Actuator	Rate Limit
Aileron	30 deg/sec
Rudder	22 deg/sec
Command Authority	**Limit**
Pilot Aileron	±10 deg
Roll SAS	±5.0 deg
Yaw SAS	±4.2 deg

4.3 Construct Unified Analysis Diagram

Those elements identified as possible contributors to PIO in Section 4.2 will now be isolated in a unified analysis diagram. The linear elements will be considered to have a multiplicative uncertainty as shown in Figure 3-2. The linear elements are the pilot gain (K_{pilot}), the roll SAS gain (K_p), the yaw SAS gain (K_r), and the interconnect ratio (K_I). The nonlinear elements (the three command limits and the two actuator rate limits) will be modeled with the equivalent gain representation of Figure 3-3 for the stability robustness analysis and with the complementary describing function representation of Figure 3-13 for the limit cycle analysis. The SIMULINK™ diagram used to define M(s) is given in Figure 4-5.

In the stability robustness analysis, the variation associated with the pilot and the variations associated with the roll and yaw SAS feedback channels can be considered as either linear variations in the pilot and feedback gains or as variations due to the saturation of the command limiters. The representation of the variations is identical in either case. Indeed, it is even possible to define a relationship in which the single variation can be considered as a combination of a variation in the linear gain combined with a variation in the equivalent gain due to limiting of the nonlinear element - although that possibility will

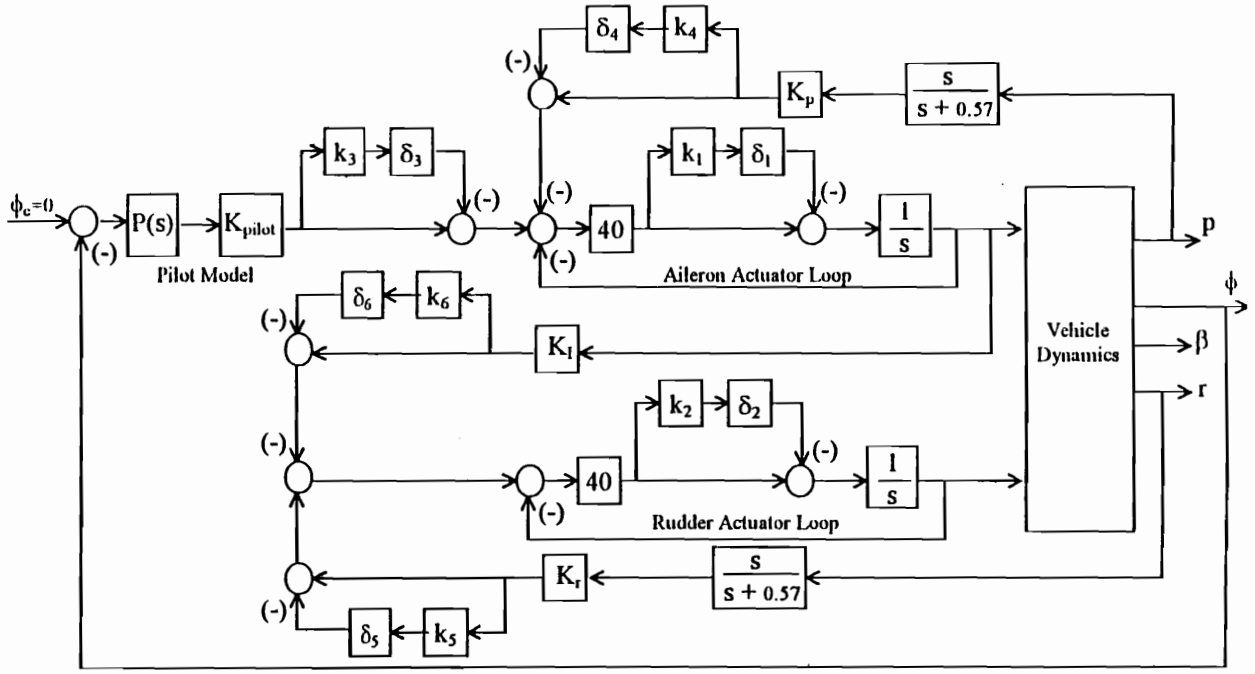

Figure 4-5. Unified Analysis Diagram for the M2-F2.

Table 4-3. *Inport/Outport* Pairs for Unified PIO Analysis.

Inport/Outport Pair	Description of Dynamic Element
1	Aileron Rate Limit
2	Rudder Rate Limit
3	Pilot Gain/Aileron Command Limit
4	Roll SAS Gain/Command Limit
5	Yaw SAS Gain/Command Limit
6	Interconnect Ratio

not be explored here. Instead, only the net effect of the variation in gain will be addressed regardless of whether the variation represents a linear or nonlinear effect.

Associated with each uncertainty is an *inport/outport* pair. The *inport/outport* pairs and the corresponding dynamic elements under consideration are listed in Table 4-3. When the *linmod* command is issued, a state-space representation of M(s) is returned having 6 inputs and 6 outputs. If it is desired to consider only a subset of the defined uncertainties, one need only to extract the relevant portions of the state-space model. If, for example, only the combined effect of an uncertain pilot gain in conjuncture with rate limiting of the aileron actuator is to be considered, then only the first and third inputs and outputs of the system M(s) are needed.

4.4 Stability Robustness Analysis

With the M-Δ construction complete, the structured singular value can be used to calculate the pertinent stability margins. As stated previously, when bounds are known to exist on a given variation, the corresponding uncertainty should be scaled to reflect this variation. If, for example, the roll SAS gain is known to vary by no more than 10% from the nominal value, then the scaling gain of 0.1 should be applied to the corresponding *inport/outport*. This scaling ensures that as δ varies from +1 to -1, the corresponding SAS gain ((1+.1δ)Kp) varies from (1- .1)Kp to (1 +.1)Kp; a variation of ±10% from the nominal gain. However since no such information is given for the M2-F2, an alternate ap-

proach is used. With all the scaling gains set to unity, the structured singular value for real parameter variations is used to estimate the single uncertainty stability margins for each of the six uncertainties.

The results of this single-variable analysis are presented in Table 4-4. A +1 or -1 in a column represents the "worst case" variation leads to an increase (+1) or decreases (-1) in the corresponding gain. A zero indicates the gain was not allowed to vary. The minimum of the structured singular value inverse ($\min(1/\mu_r)$) represents the size of the real parameter variation necessary before instability is possible. The frequency at which this minimum occurs is denoted ω_{min}. Also given in the table are the exact uncertainties (δ_{exact}) necessary to cause instability and the corresponding critical frequency (ω_{exact}). As in section 3.5.3, exact values are determined by computing the eigenvalues directly. The estimated stability margins are between 93% and 98% of the exact values.

For those uncertainties with $\min(1/\mu_r) < 1$, the scaling gains are now set equal to the single uncertainty stability margin estimates. For example, the scaling gain on the pilot gain uncertainty *import* is set to k=0.6088 because the first row of Table 4-4 indicates $\min(1/\mu_r)$ equal to 0.6088. This manipulation results in scaling the uncertainties to their single loop equivalent stability margins, with the exception of the uncertainties in the roll

Table 4-4. Single Uncertainty Stability Margins for the M2-F2.

Pilot Gain	Aileron Rate	Rudder Rate	Roll SAS	Yaw SAS	Interconnect Ratio	Minimum $(1/\mu_r)$	δ_{exact}	ω_{min} (rad/sec)	ω_{exact} (rad/sec)
1	0	0	0	0	0	.6088	.6315	5.55	5.92
0	-1	0	0	0	0	.8571	.9032	4.11	2.93
0	0	-1	0	0	0	.6848	.7285	2.65	2.28
0	0	0	-1	0	0	1.7883	1.9050	4.78	4.31
0	0	0	0	-1	0	1.0485	1.0516	2.75	2.70
0	0	0	0	0	-1	.1325	.1357	3.30	3.44

and yaw SAS gains that are left at unity. Now, the effect of varying many parameters simultaneously can be considered with increased accuracy.

The results of the stability robustness analysis for scaled parameter variations are given in Table 4-5. The stability margins given in this table represent margins that are subordinate to the single loop margins. Consider the case of varying pilot gain and the interconnect ratio simultaneously (row 5). The margin is given as 0.6586. This result means that the closed-loop system is guaranteed to remain stable as long as variations in both parameters remain below 66% of the their corresponding single loop instability values. Assuming all other uncertainties are zero, if the pilot gain does not increase by more than 0.6586*0.6088=40% and the interconnect ratio does not decrease by more than 0.6586*0.1325=9%, the closed-loop system will remain stable.

It is obvious that stability margins calculated for multiple uncertainties are greatly affected by the scaling gains. Therefore, when bounds on the model parameter variations are *not* known, this analysis can only be used to determine relative stability due to various combinations of uncertainties. Other researchers have used similar methods to reduce conservatism in structured singular value calculations [49]. With this reasoning, the results of Table 4-5 can be viewed as a sensitivity analysis.

Based upon a percentage from nominal and from the single uncertainty margins of Table 4-4, the interconnect ratio distinguishes itself as the parameter to which stability of the closed-loop system is by far the most sensitive. The pilot gain is a distant second. Since we are primarily interested in examining the stability of the system with respect to variations in the pilot model, all of the multiple uncertainty margins given in Table 4-5 include a variation in the pilot gain. The first 5 rows of Table 4-5 show the results for varying only two parameters. Again, stability of the system is strongly affected by variations in the pilot gain and the interconnect ratio (row 5). However, closed-loop stability is most sensitive to simultaneous variations in pilot gain and roll SAS gain (row 3). The next six rows (rows 6-11) show the results for varying three parameters simultaneously while

Table 4-5. Multiple Uncertainty Stability Margins for the M2-F2.

Row #	Pilot Gain	Aileron Rate	Rudder Rate	Roll SAS	Yaw SAS	Interconnect Ratio	Minimum $(1/\mu_r)$	ω_{min} (rad/sec)
1	1	-1	0	0	0	0	.6894	5.12
2	1	0	-1	0	0	0	.8196	6.30
3	1	0	0	-1	0	0	.6298	5.24
4	1	0	0	0	-1	0	.6736	5.81
5	1	0	0	0	0	-1	.6586	3.01
6	1	-1	-1	0	0	0	.6566	5.62
7	1	-1	0	-1	0	0	.5235	5.06
8	1	0	-1	0	-1	0	.5506	2.88
9	1	0	0	-1	-1	0	.4893	5.55
10	1	-1	0	0	1	0	.5559	4.51
11	1	0	-1	-1	0	0	.5879	5.62
12	1	-1	0	0	0	1	.5539	3.79
13	1	0	-1	0	0	1	.5076	3.30
14	1	0	0	-1	0	-1	.4961	5.36
15	1	0	0	0	-1	1	.4525	3.12
16	1	-1	0	-1	0	-1	.4351	5.24
17	1	-1	-1	0	0	1	.4662	3.34
18	1	0	-1	0	-1	1	.3696	3.05
19	1	-1	-1	-1	-1	1	.3277	3.08

keeping the interconnect ratio at its nominal value. The remaining rows show the results for varying pilot gain, interconnect ratio and selected combinations of other parameters.

The results for varying pilot gain, aileron rate limit, and roll SAS gain (row 7) as compared with varying pilot gain, rudder rate limit, and yaw SAS gain (row 8) for the cases of constant (rows 7 and 8) and varying (rows 16 and 18) interconnect ratios are noteworthy. When the interconnect ratio is held constant, system stability is more sensitive to variations in the aileron rate limit and roll SAS gain ($\min(1/\mu_r) = 0.52$ as opposed to 0.55). System stability is more sensitive to variations in the rudder rate limit and the yaw SAS gain when the interconnect ratio is allowed to vary ($\min(1/\mu_r) = 0.37$ compared to 0.44). Since the pilot command affects the rudder only through the interconnect ratio, this switch in sensitivity is understandable. Note also, the "worst case" direction of variation of the interconnect ratio is different for the two cases.

Another trend that can be found in Table 4-5 is that an increase in the interconnect ratio causes a decrease in the corresponding frequency. This trend is easily seen in comparing the first four rows to rows 12 through 15. A last trend to note is perhaps the most obvious. Namely, the stability margins decrease as any single parameter is added to an already existing combination. The stability margin for varying pilot gain, aileron rate limit, and roll SAS gain (0.5235) is less than the stability margin for varying only pilot gain and aileron rate limit (0.6894), or only pilot gain and roll SAS gain (0.6298).

4.5 Multivariable Describing Function Analysis

The stability robustness analysis of the previous section produced guaranteed stability bounds. That is to say, as long as the given parameters stay within the bounds, the closed-loop system will remain stable and *will not limit cycle*. However, the structured singular value analysis yields little information about the behavior of the instability when the bounds are breached. Also, since the variations of the equivalent gains representing the nonlinearities are input amplitude dependent, it is more difficult to ascertain if these bounds will be breached by the operating pilot/aircraft system. To provide further insight into the system behavior, a describing function analysis is performed to identify the existence of any limit cycles. A limit cycle can only exist when either the pilot, aircraft, or both include nonlinear elements. For the M2-F2 example, the pilot is assumed to be represented by the linear MOCM pilot while the aircraft is assumed to contain the five isolated saturation nonlinearities listed in Table 4-2.

With the system cast in the standard M-Δ form, the numerical methods of Section 3.6.2 can be used to search for the existence of limit cycles. The limit cycle search is a search for the input signals to the nonlinear elements of the form of equation (3-15) that solve the harmonic balance equation (3-17). This search can include many of the same variations as the stability robustness analysis. The results of considering all five nonlinearities in conjunction with a variation in pilot gain and a variation in the interconnect ratio will be presented here. The pilot gain and interconnect are suspected of contributing to

the oscillation tendencies as indicated by the results of the stability robustness analysis of the previous section. The results of the initial limit cycle search are given in a set of three tables. Each table contains limit cycle solutions over a range of pilot gains for a single value of the interconnect ratio.

In addition to the input signals to the nonlinear elements, which are a direct result of the solution of Equation (3-17), the magnitudes and phases of the other signals in the feedback loop may be of interest. In the case of the M2-F2, the bank angle response (ϕ) is a good indicator of oscillation severity. When other such signals are desired, they may be approximated by standard block diagram manipulation. Figure 4-6 shows the relationship between the bank angle response and the input signals to the actuator rate limiting non-linearities. With the input signals represented by,

$$x_a(t) = \alpha_a \sin(\omega t + \theta_a) \tag{4-2}$$

$$x_r(t) = \alpha_r \sin(\omega t + \theta_r) \tag{4-3}$$

The steady state bank angle output is given by,

$$\begin{aligned}\phi(t) &= \alpha_a |G_a(j\omega)| \sin(\omega t + \theta_a + \angle G_a(j\omega)) + \alpha_r |G_r(j\omega)| \sin(\omega t + \theta_r + \angle G_r(j\omega)) \\ &= \alpha_\phi \sin(\omega t + \theta_\phi)\end{aligned} \tag{4-4}$$

where G_a and G_r are as indicated in Figure 4-6, and the magnitudes and phases are to be calculated at the limit cycle solution. N_a and N_r are SIDF representations of the saturation nonlinearity (*not* the complementary dead-zone nonlinearity). The bank angle output phase and amplitude can then be given as,

$$\theta_\phi = \tan^{-1}\left(\frac{\alpha_a |G_a| \sin(\theta_a + \angle G_a) + \alpha_r |G_r| \sin(\theta_r + \angle G_r)}{\alpha_a |G_a| \cos(\theta_a + \angle G_a) + \alpha_r |G_r| \cos(\theta_r + \angle G_r)}\right) \tag{4-5}$$

$$\begin{aligned}\alpha_\phi &= \frac{\alpha_a |G_a| \sin(\theta_a + \angle G_a) + \alpha_r |G_r| \sin(\theta_r + \angle G_r)}{\sin\theta_\phi} \\ &= \frac{\alpha_a |G_a| \cos(\theta_a + \angle G_a) + \alpha_r |G_r| \cos(\theta_r + \angle G_r)}{\cos\theta_\phi}\end{aligned} \tag{4-6}$$

The bank angle results, as calculated above, are also included in the tables.

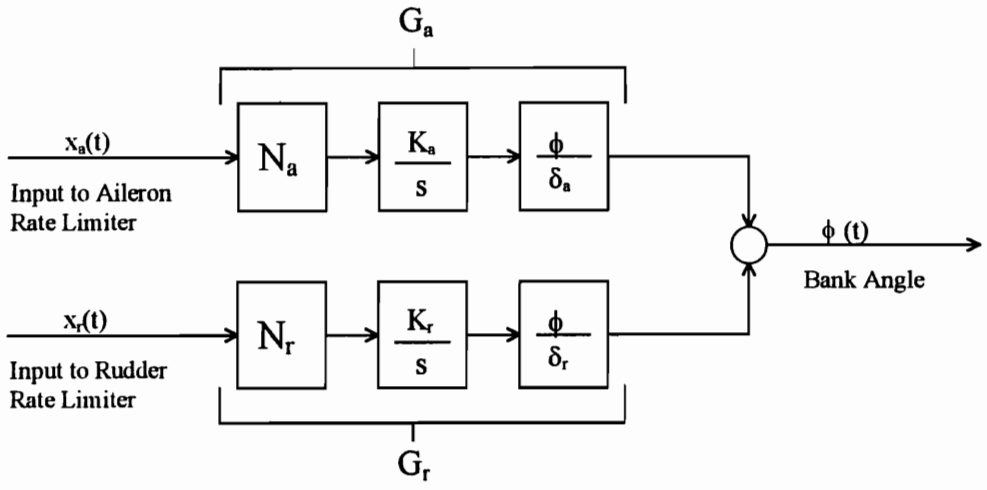

Figure 4-6. Steady-State Bank Angle Output Due to Sinusoidal Inputs.

Table 4-6 gives the results for the nominal interconnect ratio of 0.45. The table shows that limit cycle solutions exist for the given range of pilot gains. These solutions are characterized by a high degree of aileron saturation. The input to the aileron rate limiter has an amplitude between five and nine times the limit value. The only other limited saturation element is the pilot's aileron command. The commanded input is between one to two times the command limit. The remaining elements are not saturated. The solutions all oscillate at a frequency of approximately 4 rad/sec. The limit cycle solutions are predicted to be stable ($d\sigma/dA_1<0$) for pilot gains greater than or equal to 1.5 times the nominal gain. The solutions are predicted unstable at lower pilot gains. For this nominal value of the interconnect ratio, the bank angle amplitude of the predicted limit cycles is seen to be on the order of two degrees.

From the stability robustness analysis, the gain margin for varying pilot gain only was found to be 1.6. The stable limit cycles predicted in Table 4-6 exhibit soft self-excitation for pilot gains greater than this margin and hard self-excitation for pilot gains below the margin. In fact, all stable limit cycles found for the M2-F2 with MOCM pilot models

Table 4-6. Limit Cycle Solutions for Nominal Interconnect Ratio (K_I=0.45).

Pilot Gain	Input to Aileron Rate Limiter		Input to Rudder Rate Limiter		Input to Pilot Command Limiter		Input to Roll SAS Limiter		Input to Yaw SAS Limiter		Bank Angle Response		Predicted Stability
	Scaled Amplitude	Frequency (rad/sec)	Scaled Amplitude	Phase (deg)	Scaled Amplitude	Phase (deg)	Scaled Amplitude	Phase (deg)	Scaled Amplitude	Phase (deg)	Amplitude (deg)	Phase (deg)	$d\sigma/dA_1$ (Stable if < 0)
2.00	8.435	3.985	0.839	180.0	1.794	-67.2	0.450	-137.2	0.134	144.3	2.850	124.7	-0.535
1.90	8.295	4.016	0.840	179.9	1.681	-67.4	0.448	-136.9	0.134	143.5	2.815	125.0	-0.477
1.80	8.115	4.056	0.842	179.8	1.565	-67.7	0.445	-136.5	0.134	142.6	2.772	125.4	-0.414
1.70	7.870	4.111	0.844	179.7	1.444	-68.2	0.442	-136.2	0.134	141.2	2.714	125.9	-0.343
1.60	7.510	4.194	0.848	179.5	1.313	-69.0	0.437	-135.7	0.133	139.3	2.631	126.6	-0.257
1.50	6.845	4.353	0.853	179.0	1.153	-70.6	0.428	-135.0	0.131	135.6	2.481	127.5	-0.136
1.40	5.866	4.533	0.856	178.8	1.033	-73.9	0.427	-136.4	0.130	134.1	2.385	126.7	0.006
1.30	5.707	4.442	0.852	179.6	1.044	-75.5	0.447	-139.5	0.137	139.6	2.571	124.0	0.014
1.20	5.517	4.328	0.850	180.5	1.058	-77.5	0.469	-143.5	0.148	144.3	2.790	120.6	0.022
1.10	5.282	4.183	0.850	181.5	1.077	-79.8	0.492	-148.6	0.164	147.3	3.058	116.1	0.029
1.00	4.980	3.999	0.853	182.3	1.103	-82.6	0.520	-155.3	0.181	148.2	3.395	110.1	0.033

follow this trend. Namely, soft self-excitation is observed when the parameters are set such that the stability margins of the linear system representation are violated.

The effect of varying interconnect ratio on the predicted limit cycle can be seen in Tables 4-6 through 4-8. As shown in Table 4-7, lowering the interconnect ratio to 0.375 causes the bank angle amplitude and the frequency of the oscillation to increase slightly. Stable limit cycle solutions are predicted for lower pilot gains than with the nominal interconnect ratio. As the ratio is increased to 0.525 (Table 4-8), the predicted bank angle amplitude increases to approximately 10 degrees and the frequency decreases to under 3 rad/sec. For the increased interconnect ratio, stable limit cycles are predicted for the entire range of pilot gains.

A graphical representation of the limit cycle solutions for varying interconnect ratio and a fixed pilot gain of twice the nominal gain is given in Figures 4-7 and 4-8. Figure 4-7 shows the frequency of the oscillation decreases slightly as the interconnect ratio is increased. The bank angle amplitude is seen to be a minimum at the nominal interconnect ratio of 0.45. The bank angle amplitude increases slightly as the interconnect ratio is decreased from its nominal value. As the interconnect ratio is increased from the nominal value, the bank angle amplitude grows rapidly. Recall, these trends were also exhibited in the stability robustness analysis.

The corresponding input amplitudes to the nonlinear elements are shown in Figure 4-8. The input amplitudes are scaled such that values greater than unity indicate saturation of the limiters. The input amplitude to the yaw SAS command limiter and the input amplitude to the rudder rate limiter are always less than unity; indicating that these elements are not saturated during the limit cycles. The input amplitude to the aileron command limiter and the input amplitude to the aileron rate limiter are always greater than unity; indicating that these elements are saturated during the limit cycles. The input amplitude to the aileron rate limiter generally decreases with increasing interconnect ratio. The input amplitude to the aileron command limiter is a minimum at the nominal interconnect ratio and follows the same trend as the bank angle amplitude.

Table 4-7. Limit Cycle Solutions for Decreased Interconnect Ratio (K_I=0.375).

Pilot Gain	Input to Aileron Rate Limiter		Input to Rudder Rate Limiter		Input to Pilot Command Limiter		Input to Roll SAS Limiter		Input to Yaw SAS Limiter		Bank Angle Response		Predicted Stability
	Scaled Amplitude	Frequency (rad/sec)	Scaled Amplitude	Phase (deg)	Scaled Amplitude	Phase (deg)	Scaled Amplitude	Phase (deg)	Scaled Amplitude	Phase (deg)	Amplitude (deg)	Phase (deg)	$d\sigma/dA_1$ (Stable if < 0)
2.00	9.732	4.560	0.798	177.6	1.954	-62.1	0.574	-124.1	0.186	110.6	3.170	138.8	-0.363
1.90	9.615	4.575	0.798	177.5	1.844	-62.3	0.572	-124.2	0.185	110.4	3.150	138.7	-0.345
1.80	9.470	4.593	0.799	177.4	1.733	-62.7	0.570	-124.4	0.185	110.0	3.126	138.5	-0.324
1.70	9.288	4.617	0.799	177.3	1.620	-63.2	0.567	-124.6	0.184	109.5	3.095	138.4	-0.299
1.60	9.052	4.648	0.800	177.1	1.504	-63.8	0.564	-124.8	0.183	109.0	3.055	138.1	-0.268
1.50	8.730	4.692	0.800	176.9	1.384	-64.6	0.559	-125.2	0.181	108.1	2.998	137.8	-0.230
1.40	8.251	4.761	0.801	176.6	1.254	-65.9	0.551	-125.9	0.179	106.9	2.912	137.3	-0.178
1.30	7.329	4.905	0.802	175.8	1.096	-68.5	0.534	-127.1	0.174	104.3	2.738	136.2	-0.090
1.20	6.342	5.022	0.794	175.8	1.008	-72.4	0.532	-130.2	0.163	105.5	2.690	133.7	0.004
1.10	6.196	4.961	0.783	177.1	1.009	-74.1	0.555	-132.9	0.158	112.1	2.887	131.8	0.011
1.00	6.046	4.889	0.774	178.5	1.010	-76.0	0.580	-136.0	0.159	119.6	3.108	129.7	0.017

Table 4-8. Limit Cycle Solutions for Increased Interconnect Ratio (K_I=0.525).

Pilot Gain	Input to Aileron Rate Limiter		Input to Rudder Rate Limiter		Input to Pilot Command Limiter		Input to Roll SAS Limiter		Input to Yaw SAS Limiter		Bank Angle Response		Predicted Stability
	Scaled Amplitude	Frequency (rad/sec)	Scaled Amplitude	Phase (deg)	Scaled Amplitude	Phase (deg)	Scaled Amplitude	Phase (deg)	Scaled Amplitude	Phase (deg)	Amplitude (deg)	Phase (deg)	$d\sigma/dA_1$ (Stable if < 0)
2.00	5.905	2.691	0.848	177.6	5.231	-92.4	1.043	-196.7	0.120	249.2	9.907	61.3	-0.545
1.90	5.879	2.694	0.848	177.6	4.956	-92.4	1.040	-196.6	0.120	249.1	9.867	61.4	-0.485
1.80	5.849	2.697	0.848	177.7	4.679	-92.5	1.036	-196.6	0.120	248.8	9.820	61.4	-0.425
1.70	5.811	2.701	0.848	177.7	4.402	-92.5	1.032	-196.6	0.120	248.5	9.763	61.5	-0.367
1.60	5.764	2.706	0.848	177.7	4.122	-92.6	1.026	-196.5	0.120	248.2	9.692	61.5	-0.309
1.50	5.703	2.712	0.848	177.7	3.840	-92.7	1.019	-196.5	0.120	247.8	9.604	61.7	-0.250
1.40	5.620	2.720	0.848	177.7	3.554	-92.9	1.010	-196.4	0.120	247.2	9.491	61.8	-0.190
1.30	5.498	2.731	0.848	177.8	3.262	-93.0	0.998	-196.3	0.120	246.5	9.336	61.9	-0.108
1.20	5.313	2.746	0.848	177.8	2.962	-93.3	0.981	-196.1	0.119	245.4	9.118	62.1	-0.107
1.10	5.052	2.769	0.848	177.9	2.650	-93.7	0.956	-195.8	0.119	243.9	8.816	62.5	-0.105
1.00	4.660	2.804	0.847	178.0	2.321	-94.4	0.920	-195.5	0.118	241.6	8.373	63.0	-0.099

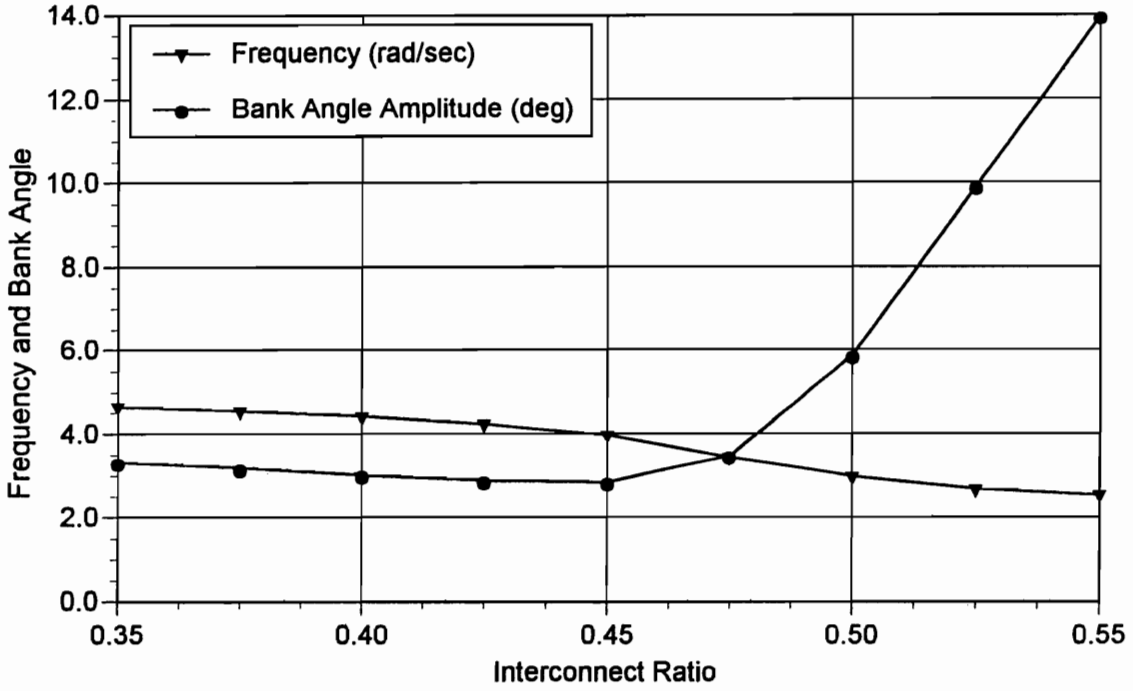

Figure 4-7. Predicted Bank Angle Amplitude and Frequency.

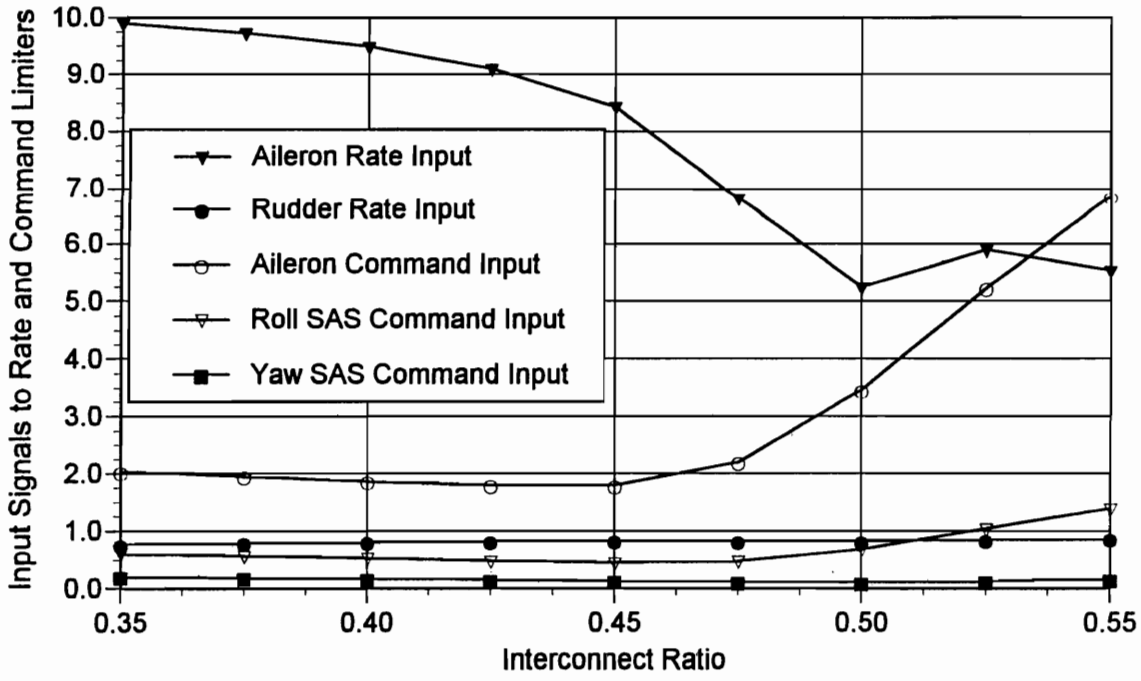

Figure 4-8. Predicted Input Amplitudes to the Saturation Elements.

All predicted limit cycles indicate rate limiting of the aileron actuator as well as limiting of the pilot's command input. The only other limiting observed was that of the roll SAS command when the interconnect ratio was increased above 0.52. This analysis shows the importance of the aileron rate limit and the pilot's command authority limit on predicted oscillation events. From this analysis, it would seem reasonable that the nonlinearities associated with the rudder rate limit and the yaw SAS could have been neglected.

The preceding analysis reveals the existence of limit cycles as solutions to the harmonic balance equation. Computer simulation of the closed-loop pilot/vehicle system can then be used to verify the results when stable limit cycles are predicted. Figure 4-9 shows the bank angle response for the three interconnect ratios given in Tables 4-6 through 4-8. The pilot gain in each case set to twice its nominal value. This plot generally confirms the predicted frequency and amplitude data given in the tables. However, for the larger interconnect ratio, the bank angle amplitude is almost twice that predicted. Keeping in mind that the describing function analysis is an approximation, and remembering the bank angle amplitude begins to increase sharply at large interconnect ratios, the discrepancy is understandable. Figure 4-10 shows the closed curve on the bank angle-bank angle rate phase plane that is characteristic of a stable limit cycle.

For a given set of parameter values, there may be more than one limit cycle solution. Table 4-9 shows another set of solutions for varying pilot gain while maintaining the nominal interconnect ratio. Figure 4-11 shows a comparison of the frequencies and bank angle amplitudes for the alternate solution set of Table 4-9 and the initial solution set of Table 4-6. The alternate solution set is characterized by large bank angle amplitudes (80 degrees) and low frequencies (1.2 rad/sec). Also, the alternate solution set shows a critical path of pilot command limiting and roll SAS limiting. Recall that the initial solution set indicates limiting of the pilot command and the aileron rate signals.

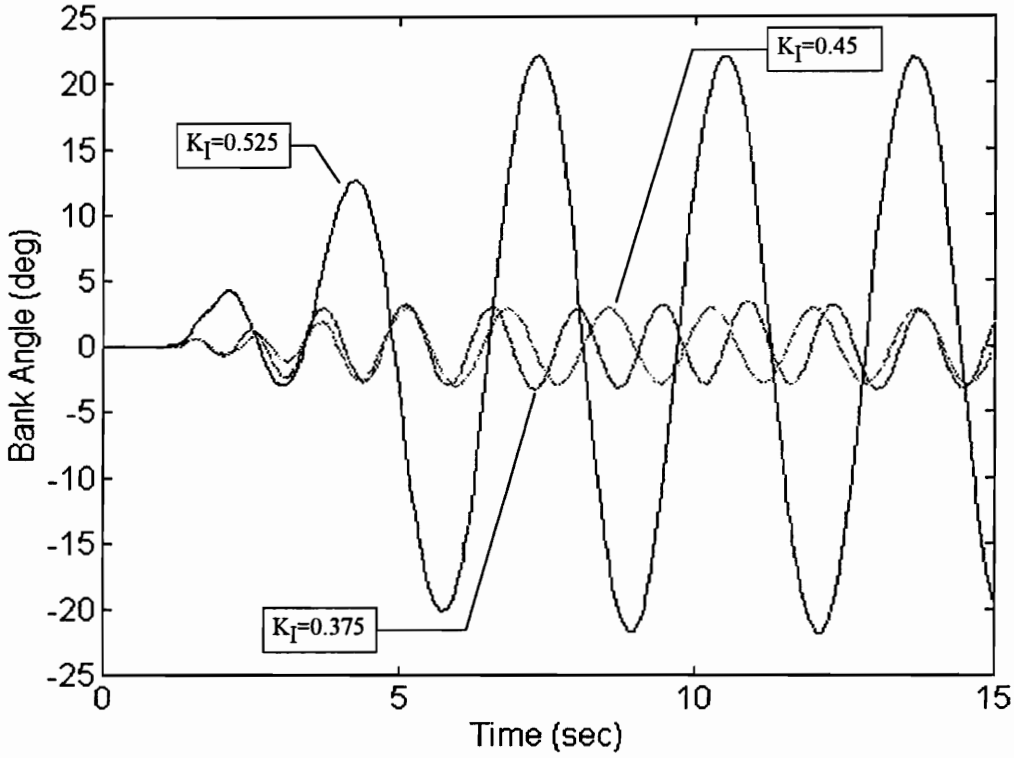

Figure 4-9. Simulated Bank Angle Response.

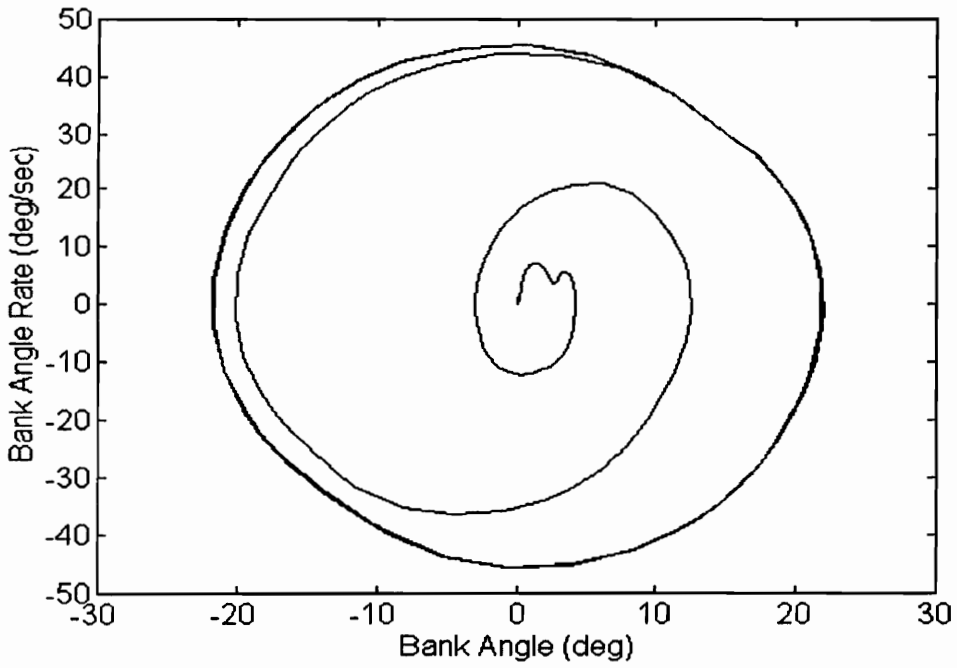

Figure 4-10. Bank Angle-Bank Angle Rate Phase Plane.

Table 4-9. Additional Limit Cycle Solutions for Nominal Interconnect Ratio (K_I=0.45).

Pilot Gain	Input to Aileron Rate Limiter		Input to Rudder Rate Limiter		Input to Pilot Command Limiter		Input to Roll SAS Limiter		Input to Yaw SAS Limiter		Bank Angle Response		Predicted Stability
	Scaled Amplitude	Frequency (rad/sec)	Scaled Amplitude	Phase (deg)	Scaled Amplitude	Phase (deg)	Scaled Amplitude	Phase (deg)	Scaled Amplitude	Phase (deg)	Amplitude (deg)	Phase (deg)	$d\sigma/dA_I$ (Stable if < 0)
2.00	0.627	1.203	0.391	165.2	12.51	-111.0	3.584	143.2	0.384	-2.6	82.43	27.8	-2.373
1.80	0.627	1.203	0.391	165.2	11.26	-111.0	3.583	143.2	0.384	-2.6	82.42	27.8	-2.379
1.60	0.627	1.203	0.391	165.2	10.01	-111.0	3.583	143.2	0.384	-2.6	82.41	27.8	-2.386
1.40	0.626	1.203	0.390	165.2	8.75	-111.0	3.582	143.2	0.384	-2.6	82.39	27.8	-2.396
1.20	0.626	1.203	0.390	165.2	7.50	-111.0	3.580	143.2	0.384	-2.6	82.36	27.8	-2.413
1.00	0.625	1.203	0.390	165.2	6.24	-111.1	3.577	143.2	0.384	-2.6	82.32	27.8	-2.441
0.80	0.624	1.202	0.389	165.2	4.99	-111.2	3.573	143.2	0.384	-2.6	82.23	27.7	-2.495
0.60	0.621	1.202	0.387	165.2	3.73	-111.3	3.562	143.1	0.383	-2.6	82.06	27.7	-2.626
0.40	0.612	1.199	0.381	165.1	2.46	-111.6	3.530	142.9	0.381	-2.7	82.50	27.4	-3.144
0.20	0.542	1.181	0.338	164.3	1.14	-114.4	3.290	141.1	0.364	-3.4	77.39	25.3	2.266
0.00	0.181	0.887	0.088	147.9	0.00	-114.4	2.086	91.3	0.339	-38.3	69.96	-31.5	12.056

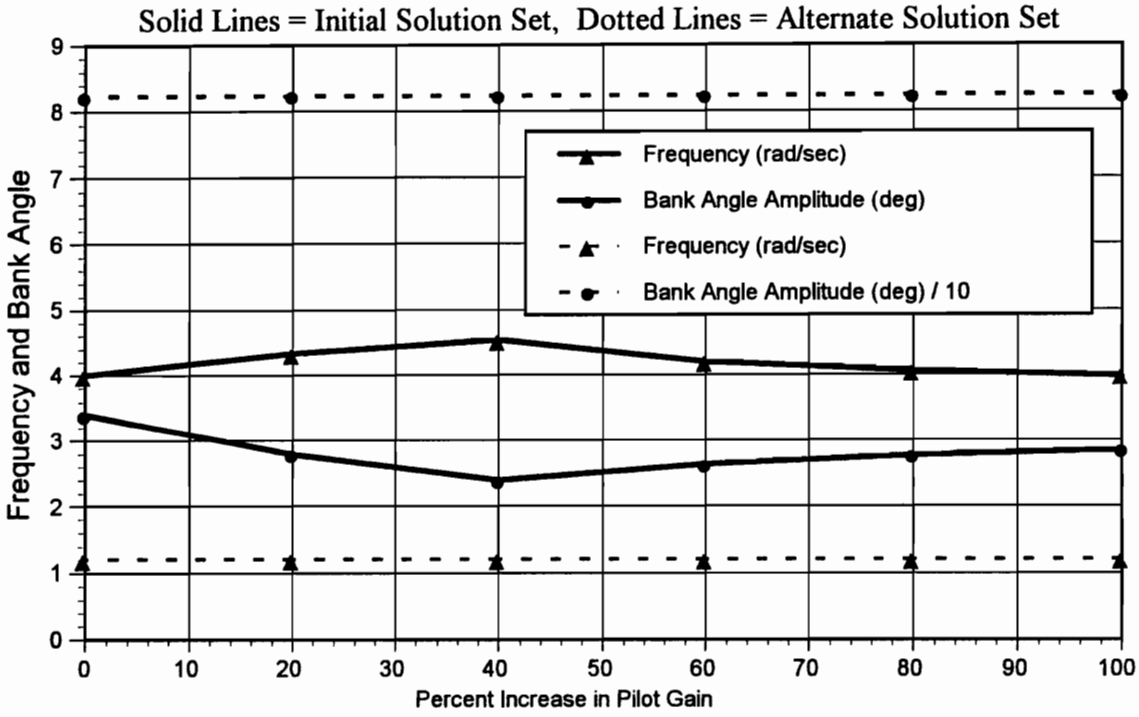

Figure 4-11. Comparison of Limit Cycle Solutions.

The alternate solution values agree much better with the flight data that indicates bank angle amplitudes greater than 50 degrees at a frequency of approximately 1.6 rad/sec. The NASA six-degree-of-freedom simulation data for aileron only pilot control indicates bank angle amplitudes near 80 degrees at a frequency of 1.3 rad/sec [6]. These values were also confirmed in pilot-in-the-loop simulations at Virginia Tech. While these values agree well with those in Table 4-9, a computer simulation of this predicted limit cycle could not be confirmed using an analytical pilot model. The phenomena of hard self-excitation is the suspected culprit.

4.6 Summary

The stability robustness analysis of the M2-F2 confirmed that the interconnect ratio, aileron rate limit, and pilot gain have a significant affect on the closed-loop system stability. The analysis also indicates rudder rate limiting has an impact. However, no pilot rudder input is considered and therefore, it is unlikely that the rudder rate limit will be reached. In particular, it was shown that closed-loop stability is very sensitive to the value of the interconnect ratio.

The describing function analysis shows that self-sustaining oscillations of the pilot/aircraft system are possible for parameter variations within the range of interest. Furthermore, the character of these oscillations changes when the parameters are varied. These trends were established through both the stability robustness and the limit cycle analyses. The predicted oscillations that could be confirmed in unmanned simulations (i.e., computer simulations containing analytical pilot models) do not agree well with those experienced in flight. However, an alternative set of harmonic balance solutions, that could not be confirmed using unmanned simulations, did result in characteristics very close to those experienced in flight and in manned simulation studies at NASA and at VPI.

5 Conclusions and Recommendations

The most significant contribution of this research is the unification of stability robustness and multivariable describing function analysis methods to examine the stability of closed-loop systems with isolated nonlinear elements. A structured approach is developed that allows the limit cycle behavior of a nonlinear system to be examined based on the unified analysis diagram. This method has strong ties with the well established framework of stability robustness methods. When applied to the study of PIO, this analysis theory shows significant promise and warrants continued development. It can handle many simultaneous dynamic effects in a systematic way and can be used to isolate any combination of dynamic elements that are suspected contributors to the occurrence of PIO.

The M2-F2 example demonstrates how several individual dynamic effects can be analyzed simultaneously. In this case, the combined effect of five separate nonlinearities and two linear parameter variations are studied. While the PIO tendency of the M2-F2 is most likely caused by poor flying qualities, a unified PIO analysis shows exactly which dynamic elements of the aircraft couple with the pilot dynamics to cause oscillations. The analysis results show the PIO amplitude and frequency that occurred during flight testing and piloted simulation of the M2-F2 can be accurately predicted assuming a MOCM pilot model and simultaneous limiting in the pilot command and roll SAS feedback channels.

However, two distinct families of limit cycle solutions were obtained using the MOCM pilot model. The lower frequency (1.2 rad/sec) solution family agrees well with the flight test and piloted simulation data. However, only the higher frequency (4 rad/sec) solution family could be confirmed with unmanned computer simulations. The oscillation frequencies for the two families differ by a factor of approximately three. That is, one family appears to be a superharmonic of the other. It is possible that modification to the MOCM model, or use of a different pilot model, might predict a single set of limit cycle solutions that can be duplicated in unmanned simulations and that agree well with the flight test and piloted (manned) simulation data. Furthermore, the resulting behavior of a system for

which more than one stable limit cycle solution is predicted should be considered in future research. The use of alternate describing functions, such as the two sinusoid input describing function (TSIDF), may yield some insight into understanding the behavior of systems for which the SIDF predicts multiple stable limit cycle solutions [40].

Another remaining research question, possibly related to the issue of multiple limit cycle solutions, focuses on the existence of soft and hard self-excitations of predicted limit cycles. A hard self-excitation requires application and removal of an external input to yield a sustained oscillation. Although both random and deterministic input signals of various waveforms were employed, none of the limit cycle solutions that agreed with the flight test data could be confirmed in unmanned simulations. Continued investigation of the hard self-excitation phenomenon is also important because it might shed light on the fact that some PIOs occur even after the aircraft has been in the fleet for several years.

A final remaining research question relates to the study of which pilot model parameters should be varied and to what degree they should be varied. Although not reported here, variations in pilot gain, time delay, and lead/lag time constants were studied during the course of this research. While pilot gain variations seemed to provide the best PIO predictions, there is sufficient evidence to warrant further investigation of other parameters. At this point, it seems logical that variations in pilot gain and time delay will figure prominently in future analyses. However, more research needs to be conducted to determine extent of the variations to consider.

Since acceptable ranges of the parameter variations have not yet been established, it would be premature at this point to make any concrete assertion as to PIO proneness of any single vehicle based on the current analysis. Analysis of other known PIO-resistant and PIO-prone aircraft is needed to establish more definite design guidelines. Unfortunately, there is no adequate database of the Category II and Category III PIOs at which this research is aimed.

References

1. Vincenti, W. G., "How Did It Become 'Obvious' That an Airplane Should Be Inherently Stable?," *Invention and Technology*, Spring Summer, 1988, pp. 50-56.

2. Military Standard, Flying Qualities of Piloted Aircraft, MIL-STD-1797A, 30 Jan. 1990.

3. Anderson, S. B., "Lessons Learned From an Historical Look at Flight Testing," NASA Tech Briefs ARC-13330, 1995.

4. Braybrook, R., "Too Much Mario and Sonic; Not Enough Orville and Wilbur?," *Air International*, Feb. 1994.

5. McRuer, D. T., "Pilot-Induced Oscillations and Human Dynamic Behavior," Systems Technology, Inc., Technical Report No. 2494-1, October 1994.

6. Kempel, R. W., "Analysis of a Coupled Roll-Spiral-Mode, Pilot-Induced Oscillation Experienced With the M2-F2 Lifting Body," NASA TN D-6496, September 1971.

7. Mitchell, D. G., and Hoh, R. H., "Development of a Unified Method to Predict Tendencies for Pilot-Induced Oscillations," Hoh Aeronautics Inc., Technical Report No. 1043-1, January 1995.

8. Dornheim, M. A., "Report Pinpoints Factors Leading to YF-22 Crash," *Aviation Week & Space Technology*, Nov. 9, 1992, pp. 53-54.

9. A'Harrah, R. C., "An Alternate Control Scheme for Alleviating Aircraft-Pilot Coupling," Paper No. 94-3673, AIAA Guidance, Navigation and Control Conference, Scottsdale, AZ, Aug. 1994, pp. 1194-1201.

10. McKay, K., "Summary of an AGARD Workshop on Pilot Induced Oscillation," Paper No. 94-3668, AIAA Guidance, Navigation and Control Conference, Scottsdale, AZ, Aug. 1994, pp. 1151-1161.

11. Anderson, M. R., "Standard Optimal Pilot Models," Paper No. 94-3627, AIAA Guidance, Navigation, and Control Conference, Scottsdale, AZ, Aug. 1994.

12. Doman, D. B., "Interactive Flying Qualities Toolbox for MATLAB® User's Guide," WL-TR-95-3070, August 1995.

13. Bjorkman, E. A., Silverthorn, J. T., and Calico, R. A., "Flight Test Evaluation of Techniques to Predict Longitudinal Pilot Induced Oscillations," Paper 86-2253, AIAA Guidance, Navigation, and Control Conference, Williamsburg, VA, Aug. 1986, pp. 967-975.

14. Hess, R. A. and Kalteis, R. M., "Technique for Predicting Longitudinal Pilot-Induced Oscillations," *Journal of Guidance, Control, and Dynamics*, Vol. 14, No. 1, Jan.-Feb. 1991, pp. 198-204.

15. Hofmann, L. G., Shah, K. V., and Graham, D., "Analysis of Limited Authority Manual Control Systems," AFFDL-TR-71-6, July 1971.

16. Hirsch, D. L. and McCormick, R. L., "Experimental Investigation of Pilot Dynamics in a Pilot-Induced Oscillation Situation," *Journal of Aircraft*, Vol. 3, No. 6, Nov.-Dec. 1966, pp. 567-573.

17. Neal, T. P., and Smith, R. E., "An In-Flight Investigation to Develop Control System Design Criteria for Fighter Airplanes," AFFDL-TR-70-74, Vol. I, December 1970.

18. Smith, R. H., "A Theory for Longitudinal Short Period Pilot Induced Oscillations," AFFDL-TR-77-57, June 1977.

19. McRuer, D. T., and Jex, H. R., "A Review of Quasi-Linear Pilot Models," *IEEE Transactions on Human Factors in Electronics*, Vol. HFE-8, No. 3, Sept. 1967, pp. 231-249.

20. Smith, R. H. and Geddes, N. D., "Handling Quality Requirements for Advanced Aircraft Design: Longitudinal Mode," AFFDL-TR-78-154, Aug. 1979.

21. Hess, R. A., "A Model-Based Investigation of Manipulator Characteristics and Pilot/Vehicle Performance," *Journal of Guidance, Control, and Dynamics*, Vol. 6, No. 5, Sept.-Oct. 1983, pp. 348-354.

22. Hess, R. A., "Analysis of Aircraft Attitude Control Systems Prone to Pilot-Induced Oscillations," *Journal of Guidance, Control, and Dynamics*, Vol. 7, No. 1, Jan.-Feb. 1984, pp. 106-112.

23. Kleinman, D. L., Baron, S., and Levison, W. H., "An Optimal Control Model of Human Response, Part I: Theory and Validation," *Automatica*, Vol. 6, Pergamon Press, Ltd., 1970, pp. 357-369.

24. Anderson, M. R., and Schmidt, D. K., "Closed-Loop, Pilot/Vehicle Analysis of the Approach and Landing Task," *Journal of Guidance, Control, and Dynamics*, Vol. 10, No. 2, March-April 1987, pp.187-194.

25. Bacon, B. J., and Schmidt, D. K., "An Optimal Control Approach to Pilot/Vehicle Analysis and the Neal-Smith Criteria," NASA CR-170416, April 1984.

26. Waszak, M. R., and Schmidt, D. K., "Analysis of Flexible Aircraft Longitudinal Dynamics and Handling Qualities," NASA CR-177943, June 1985.

27. Anderson, M. R., and Page, A. B., "Unified Pilot-Induced Oscillation Theory," WL-TR-96-3030, December 1995.

28. Graham, D. and McRuer, D., "Retrospective Essay on Nonlinearities in Aircraft Flight Control," *Journal of Guidance, Control, and Dynamics*, Vol. 14, No. 6, Nov.-Dec. 1991, pp. 1089-1099.

29. Smith, R., "Predicting and Validating Fully-Developed PIO," Paper No. 94-3669, AIAA Guidance, Navigation and Control Conference, Scottsdale, AZ, Aug. 1994, pp. 1162-1166.

30. Davidson, J. B. and Schmidt, D. K., "Modified Optimal Control Pilot Model for Computer-Aided Design and Analysis," NASA TM-4384, Oct. 1992.

31. Manning, M. K. and Banda, S. S., "Algorithm to Obtain M-Δ Form for Robust Control," International Conference on Systems Engineering, Dayton, OH, Aug 24-26, 1989.

32. Yeh, H. H., Ridgely, D. B., and Banda, S. S., "Nonconservative Evaluation of Uniform Stability Margins of Multivariable Feedback Systems," *Journal of Guidance, Control, and Dynamics*, Vol. 8, No. 2, March-April 1985, pp. 167-174.

33. Doyle, J. C., "Analysis of Feedback Systems with Structured Uncertainties," IEE Proc., Vol. 129, Pt. D, No. 6, Nov. 1982, pp. 242-250.

34. Jones, R. D., "Structured Singular Value Analysis for Real Parameter Variations," Paper No. 87-2589, AIAA Guidance, Navigation and Control Conference, Monterey, CA, Aug. 1987, pp. 1424-1432.

35. Manning, M. K., and Banda, S. S., "Approximate Structured Singular Value Computation via Frobenius Norms," International Conference on Systems Engineering, Dayton, OH, Aug 24-26, 1989.

36. Osborne, E. E., "On Pre-Conditioning of Matrices," *Journal of the Association for Computing Machinery*, Vol. 7, 1960, pp. 338-345.

37. Anderson, M. R., and Schmidt, D. K., "An Uncertainty Model for Saturated Actuators," American Control Conference, Pittsburgh, PA, June 1989.

38. Kapasouris, P. and Athans, M., "Multivariable Control Systems with Saturating Actuators Antireset Windup Strategies," American Control Conference, Boston, MA, June 1985, pp. 1579-1584.

39. Safanov, M. G., "Stability Margins of Diagonally Perturbed Multivariable Feedback Systems," IEE Proc., Vol. 129, Pt. D, No. 6, Nov. 1982. pg. 251-256.

40. Gelb, A. and VanderVelde, W. E., *Multiple Input Describing Functions and Nonlinear System Design*, McGraw Hill Book Co., 1968.

41. Graham, D. and McRuer, D., *Analysis of Nonlinear Control Systems*, John Wiley & Sons, Inc., 1961.

42. Ogata, K., *Modern Control Engineering, Second Edition*, Prentice Hall, Inc., 1990.

43. Mees, A., "Describing Functions, Circle Criteria, and Multiple-Loop Feedback Systems," Proc. IEE, Vol. 120, No. 1, Jan. 1973, pp. 126-130.

44. Gray, J. O. and Nakhla, N. B., "Prediction of Limit Cycles in Multivariable Nonlinear Systems," IEE Proc., Vol. 128, Pt. D, No. 5, Sept. 1981, pp. 233-241.

45. Gray, J. O. and Taylor, P. M., "Computer Aided Design of Multivariable Nonlinear Control Systems using Frequency Domain Techniques," *Automatica*, Vol. 15, 1979, pp. 281-297.

46. Chang, H. C., Pan, C. T., Huang, C. L., and Wei, C. C., "A General Approach for Constructing the Limit Cycle Loci of Multiple-Nonlinearity Systems," *IEEE Transactions on Automatic Control*, Vol. AC-32, No. 9, Sept. 1987, pp. 845-848.

47. Pillai, V. K., and Nelson, H. D., "On an Extension of the Describing Function Method," American Control Conference, Atlanta, GA, June 1988, pp. 2168-2173.

48. McRuer, D. T., and Schmidt, D. K., "Pilot-Vehicle Analysis of Mulit-Axis Tasks," Paper No. 87-2538-CP, AIAA Guidance, Navigation and Control Conference, Monterey, CA, Aug. 1987.

49. Kelly, J. H., and Arnold III, W. F., "Application Issues in μ Analysis," American Control Conference, Seattle, Washington, June 1995, pp. 3000-3001.

Vita

Anthony B. Page was born in Pound, Virginia on December twenty-six, nineteen hundred sixty-seven. After graduating Pound High School in 1986, he entered the College of Engineering at Virginia Tech. While working on his B.S. in Aerospace Engineering, the author gained practical experience working in the Vehicle Control Systems Branch at NASA-Marshall Space Flight Center as part of the Co-operative Education Program. The author received B.S., M.S., and Ph.D degrees in Aerospace Engineering at Virginia Tech in 1991, 1993, and 1996 respectively.

The author is a member of the American Institute of Aeronautics and Astronautics, the honor society of Phi Kappa Phi, and Sigma Gamma Tau, the national honor society in aerospace engineering. Dr. Page is currently a Research Associate with the Department of Aerospace Engineering at Virginia Tech, but will soon begin a career at the Naval Air Warfare Center Aircraft Division at the Naval Air Station in Patuxent River, Maryland.